UNIVERZITA KARLOVA

Přírodovědecká fakulta

Studijní program: Biochemie

Bc. Zuzana Janáčková

Mechanismus regulace cyklin-dependentní kinasy 16 prostřednictvím komplexu cyklin Y/14-3-3

Regulatory mechanism of the cyclin-dependent kinase 16 through the cyclin Y/14-3-3 complex

DIPLOMOVÁ PRÁCE

Vedoucí práce: prof. RNDr. Tomáš Obšil, Ph.D.

Konzultant: Mgr. Klára Kohoutová

Praha 2023

Prohlášení

Prohlašuji, že jsem závěrečnou práci zpracovala samostatně a že jsem uvedla všechny použité informační zdroje a literaturu. Tato práce ani její podstatná část nebyla předložena k získání jiného nebo stejného akademického titulu.

Praha 25. srpna 2023 .....

Zuzana Janáčková

Poděkování

First of all, I would like to thank my supervisor, Tomáš Obšil, for giving me the opportunity to work in his research group. I greatly appreciate his advice and expertise during the development of my master's thesis. I would also like to thank Veronika Obšilová for allowing me to use her laboratory, for her help, support and kind words. I would also like to express my gratitude to my consultant Klára Kohoutová for her patience, help and advice, and for all the time she devoted to this project. Another thank you goes to Dalibor Košek for his help with the refinement, for the explanation of the principles of protein crystallography and for all the useful advice, to Karolína Honzejková for all her help, advice and support, to Raju Mandal for his patience in teaching me how to use the Watrex chromatography machine and to all the members of the Laboratory of Biophysical Chemistry of Protein Complexes and the Laboratory of Structural Biology of Signalling Proteins for the friendly environment and sharing of their valuable experience. Finally, I would like to thank my family and friends for their help, understanding and support.

Abstrakt

CDK16 je cyklin-dependentní kinasa podílející se na regulaci buněčného cyklu. Podílí se především na procesech růstu neuritů, regulaci axonálního transportu a vývoji spermií. Hraje také roli v progresi XLID (z angl. X-linked intellectual disability) a spolu se svým aktivačním partnerem cyklinem Y ve vývoji a progresi různých typů rakoviny. CDK16 a cyklin Y by proto mohly představovat potenciální nové terapeutické cíle.

CDK16 i cyklin Y jsou strukturně atypické mezi podobnými proteiny a mechanismus aktivace CDK16 cyklinem Y zatím není známý. Z předchozích studií však vyplývá, že interakce mezi CDK16 a cyklinem Y vyžaduje předchozí interakci cyklinu Y s 14-3-3 proteiny. Pro interakci cyklinu Y s 14-3-3 proteiny je nutná fosforylace jeho 14-3-3 vazebných míst, S100 a S326. S cílem zjistit přesný mechanismus aktivace CDK16 jsme se rozhodli blíže charakterizovat interakci mezi CDK16, cyklinem Y a 14-3-3 proteiny.

Pro charakterizaci interakcí mezi CDK16, cyklinem Y a 14-3-3 proteiny byla využita řada biofyzikálních metod, včetně fluorescenční anisotropie, nativní gelové elektroforézy, gelové permeační chromatografie a proteinové krystalografie. Pomocí nativní elektroforézy a gelové permeační chromatografie byla potvrzena tvorba binárních pCCNY–14-3-3 a ternárních CDK16–pCCNY–14-3-3 proteinových komplexů. Pomocí upřesnění krystalové struktury byla zjištěna detailní struktura vazebného rozhraní 14-3-3 vazebného motivu cyklinu Y v komplexu s 14-3-3 γ. Všechny výsledky prezentované v této práci mohou být použity jako první krok k pochopení struktury a interakcí v proteinovém komplexu CDK16–pCCNY–14-3-3.

Klíčová slova: CDK16; cyklin Y; 14-3-3 proteiny; krystalografie

Abstract

CDK16 is a cell-cycle-related cyclin-dependent kinase that functions primarily in neurite growth processes, axonal transport regulation and sperm development. It also plays a role in the progression of X-linked intellectual disability and, together with its activating partner cyclin Y, in the development and progression of various types of cancer. Consequently, CDK16 and cyclin Y could represent potential new therapeutic targets.

Both CDK16 and cyclin Y are structurally atypical among similar proteins, and the mechanism of activation of CDK16 by cyclin Y is unclear. However, it is clear from recent studies that the interaction between CDK16 and cyclin Y requires the prior interaction of cyclin Y with 14-3-3 proteins. In addition, for cyclin Y to interact with 14-3-3 proteins, its phosphorylation on the S100 and S326 binding sites of 14-3-3 is required. To investigate the mechanism of activation of CDK16 by cyclin Y, we decided to characterize the interaction between CDK16, cyclin Y and 14-3-3 proteins in detail.

The interaction between CDK16, cyclin Y and 14-3-3 proteins was characterized using biophysical methods including fluorescence anisotropy measurements, native electrophoresis, size exclusion chromatography and protein crystallography. The formation of binary pCCNY–14-3-3 and ternary CDK16–pCCNY–14-3-3 protein complexes was confirmed by native electrophoresis and size exclusion chromatography. The detailed structure of the binding interface of the 14-3-3 binding motif of CCNY in complex with 14-3-3 γ was provided by refinement of the crystal structure of the complex. All results presented in this thesis can be used as a first step towards understanding the structure and interactions in the CDK16–pCCNY–14-3-3 protein complex.

Key words: CDK16; cyclin Y; 14-3-3 proteins; crystallography

Contents

Abbreviations

AAK1 ..... AP2-associated kinase 1
ADP ..... Adenosine diphosphate
AMP ..... adenosine 5'-monophosphate
ASK ..... Apoptosis signal-regulating kinase 1
ATP ..... Adenosine triphosphate
CaMKK .Calcium/calmodulin-dependent protein kinase kinase
CBD ..... Cyclin box domain
CCNA ..... Cyclin A
CCNY ..... Cyclin Y
CDK ..... Cyclin-dependent protein kinase
CDK16 ..... Cyclin-dependent kinase 16
CKIs ..... Cyclin-dependent kinase inhibitors
CV ..... Column volume
DEAE ..... Diethylaminoethyl
DNA ..... Deoxyribonucleic acid
DNase I ..... Deoxyribonuclease I
DTT ..... Dithiotreitol
ERK ..... Extracellular signal-regulated kinases
FPLC ..... Fast protein liquid chromatography
GST ..... Glutathione S-transferase
HBS ..... HEPES-buffered saline
HEPES ... 4-(2-hydroxyethyl)-1-piperazineethanesulfonic acid
IPTG ..... Isopropyl β-D-1-thiogalactopyranoside
LB ..... Lysogenia Broth
MEK ..... Mitogen-activated protein kinase kinase
OD ..... Optical density

PAGE ..... Polyacrylamide gel electrophoresis
PBS ..... Phosphate-buffered saline
pCCNY ..... Phosphorylated cyclin Y
PDB ..... Protein Data Bank
PKA ..... Protein kinase A
PMSF ..... Phenylmethylsulfonyl fluoride
SDS ..... Sodium dodecyl sulfate
TBE ..... Tris-borate-EDTA
TCEP ..... Tris(2-carboxyethyl)phosphine
tRNA ..... Transfer ribonucleic acid
XLID ..... X-linked intellectual disability

Introduction

During human growth, a single zygote becomes an adult composed of around $3 \cdot 10^{13}$ cells through the process of cell division. [1] In the early stages of development, cell division is active in most of the body's tissues. In adult organisms, on the other hand, most cells are in a quiescent, non-dividing state. As a result, cell division and the entire cell cycle must be tightly regulated to take place in the right place at the right time. Otherwise, unregulated cell division can lead to cancer. [2]

The main intrinsic mechanism controlling, regulating and modulating the cell cycle are cyclin-dependent protein kinases and their binding partners, cyclins. Today, many cyclin-dependent kinases are known, and even more cyclins whose activities and roles vary during the cell cycle. Cyclin-dependent kinases modulate the activity of other proteins by phosphorylation, one of the most widespread post-translational modifications that can strongly affect protein conformation and activity. Without cyclin-dependent kinases, the cell cycle cannot proceed physiologically. [2, 3]

CDK16 is an atypical cyclin-dependent kinase, which differs from other CDKs by its N- and C-terminal extensions and the replacement of a single amino acid in the cyclin-binding C-helix. CDK16 is involved in neurite outgrowth, vesicle trafficking and synaptic transmission, and is essential for proper development of spermatozoa. It also plays a role in the development of X-linked intellectual disability. [4, 5]

Until recently, CDK16 was considered an orphan kinase, with no known cyclin partner. Recent publications clearly show that CDK16's interaction partner is cyclin Y (CCNY), whose structure also differs from the typical cyclin structure by containing only one cyclin box fold instead of two. It has also been verified that the interaction between CDK16 and CCNY requires the phosphorylation of CCNY (pCCNY) and the presence of 14-3-3 proteins. The exact mechanism of this interaction is not yet well understood. [6, 5] Therefore, the aim of the project solved in our laboratory is to further investigate the potential new mechanism of CDK16 activation through the formation of the CDK16-pCCNY-14-3-3 ternary complex. The aim of this thesis is to characterize the formation of the pCCNY–14-3-3 and CDK16–pCCNY–14-3-3 complexes.

To achieve this goals, various biophysical methods are used. Fluorescence anisotropy is used to study the interaction of a labelled peptide molecule with a protein,

and to measure the protein's affinity for the peptide. Native electrophoresis visualizes the formation of protein complexes. The size exclusion chromatography enables to characterize the binary and ternary complexes. Finally, X-ray crystallography is used to create a model of whole molecules and their active sites, also in complex with other peptides or proteins. All these methods can help shed light on the unknown details of CDK16's activation mechanism.

Chapter 1

Theoretical Part

1.1 Cell cycle

Cell division is a crucial process for the development, life and reproduction of all organisms. In eukaryotes, cell division is part of the complex and well-organized process called the cell cycle (Fig. 1). [2] The standard cell cycle consists of four phases: synthesis (S phase), where the chromosomes are replicated and the genetic information of the cell is doubled, mitosis (M phase), where the chromosomes are divided into two genetically identical daughter cells, and two gap phases between them (G_1 phase between the M and S phase, G_2 phase between the S and M phase). Under specific conditions (starvation, inhibition), the cell can undergo a reversible transition from phase G_1 to phase G_0 (also known as the quiescent state). [7]

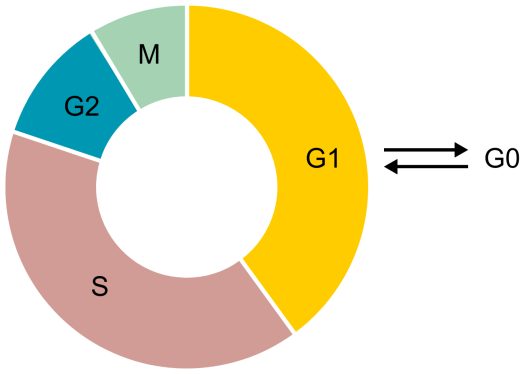

Figure 1. Scheme of the cell cycle and its main phases. *During the G_1 phase, the cell can (reversibly) enter the G_0 phase. During S phase takes place the replication of the genome. After G_2 phase, the cell enters M phase and is divided to two daughter cells. Adapted from [2].*

As the precise function of the cell cycle is critical for the existence of the organism, the whole process is strictly regulated and controlled by many different mechanisms:

1. Extrinsic regulation ensures that cell division occurs at the right time and in the right place, in coordination with other cells of the organism, and based on outer conditions (e.g., energy and nutrients supply). It is based on a large scale of growth factors, cytokines, and cell–cell interaction molecules, as well as the presence or absence of pro- apoptotic signals. The regulation occurs at two levels: for the cell cycle to proceed, the antimitogenic signals (e.g., the pro- apoptotic signals) must not be present, and the sufficient amount of the mitogenic signals (growth factors and cytokines) must be produced. [8, 2]

2. Intrinsic regulation contains three main cell-cycle checkpoints that are responsible for ensuring that each earlier process has been completed before the cell moves on to the next phase of the cycle. The first checkpoint, G_1 or the restriction checkpoint, controls the presence of the necessary outer growth factors, appropriate cell size, the availability of nutrients, and no detected DNA damage. The G_2/M checkpoint is activated in the event of incomplete or improper DNA replication (mitosis can occur only if all chromosomes were completely replicated) or other DNA damage. The metaphase checkpoint or the spindle checkpoint stops the transition of mitosis to anaphase when the chromosomes are not properly attached to the mitotic spindle during metaphase. [9, 10]

The proper function and regulation of the cell cycle are crucial, where dysregulation can cause many diseases, including cancer. [2] Due to the accumulation of mutations, cancer cells are capable of producing their own mitogenic signals and, at the same time, reacting defectively to outer antimitogenic signals. This leads to uncontrolled proliferation and, together with genomic and chromosomal instability, to the formation and progression of tumors. [11]

The main components that drive and regulate the cell cycle are cyclin-dependent protein kinases (CDKs) and cyclins that bind to and activate CDKs. In general, the catalytic subunit of the CDK without cyclin is inactive. When cyclin binds, the conformation of CDK changes and enables catalytic activity. In animal cells, many different cyclins and CDKs act in different combinations at specific time points in the cell cycle. The activity of specific CDKs oscillates during the cell cycle (Fig. 2 on page 19), it is regulated by phosphorylation or dephosphorylation of CDKs, periodic synthesis of CDKs and cyclins, controlled degradation of cyclins, and the presence of CDK inhibitors (CKIs). These regulatory mechanisms ensure proper functioning of the whole cell cycle. [3]

1.1.1 Protein kinases

Protein kinases catalyze the transfer of the γ-phosphoryl group of the nucleoside triphophate (usually ATP) to a particular amino acid residue in the target protein.

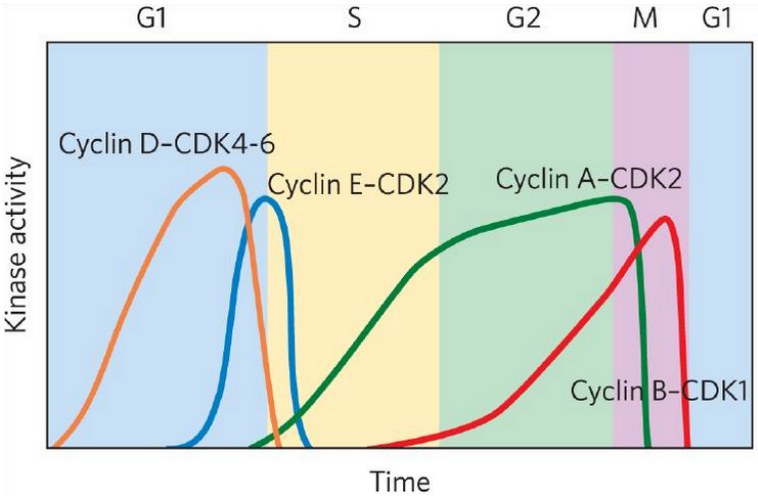

Figure 2. The changing activities of different CDK and cyclin combination during the cell cycle. *Cyclin D-CDK4–6 activity increases through the G_1 phase with the fast decrease at the ending of G_1, where cyclin E-CDK2 has the highest activity at the G_1 and S phase boundary. Cyclin A-CDK2 activity rises through S and G_2 phase and drops in the M phase, where cyclin B-CDK1 peaks. Retrieved from [3].*

In the human genome, there are more than 500 protein kinases that usually phosphorylate the –OH group of serine, threonine, or tyrosine residues (although His- or Asp/Glu-specific kinases exist, too). [3, 2] The oxygen atoms of the phosphate group can form hydrogen bonds with the surrounding hydrogen atoms (e.g., the charged guanidinium group of an Arg residue) and also repel the other charged groups due to the two negative charges. When phosphorylation occurs in a region important for protein structure, it can significantly change the conformation of the whole protein and have a dramatic effect on its activity. Regulation via phosphorylation is complex. For regulation, the presence of consensus sequences for the individual protein kinases, the structure of the whole protein (which allows the access to the target residue), and the proximity of other phosphorylated residues are important. [3]

The structure of the about 270 amino acid long catalytic domain of Ser/Thr- and Tyr-specific protein kinases is conserved and consists of two main lobes with an active site that forms a cleft between them (Fig. 3 on page 20). The ATP molecule binds to the cleft, with the γ-phosphate oriented outward.

The small N-terminal lobe formed by five antiparallel β-sheets and one long α-helix (named C-helix) forms a binding site for ATP. There is a glycine-rich motif G-X-G-X-X-G-X-V between the β-sheets one and two. The conserved glycines allow for the short distance between the nucleotide and the peptide backbone. The invariant lysine (Lys72 in PKA) from strand three contributes to the correct stereochemical orientation of ATP. Its position is secured by the salt bridge to Glu91 in the C-helix.

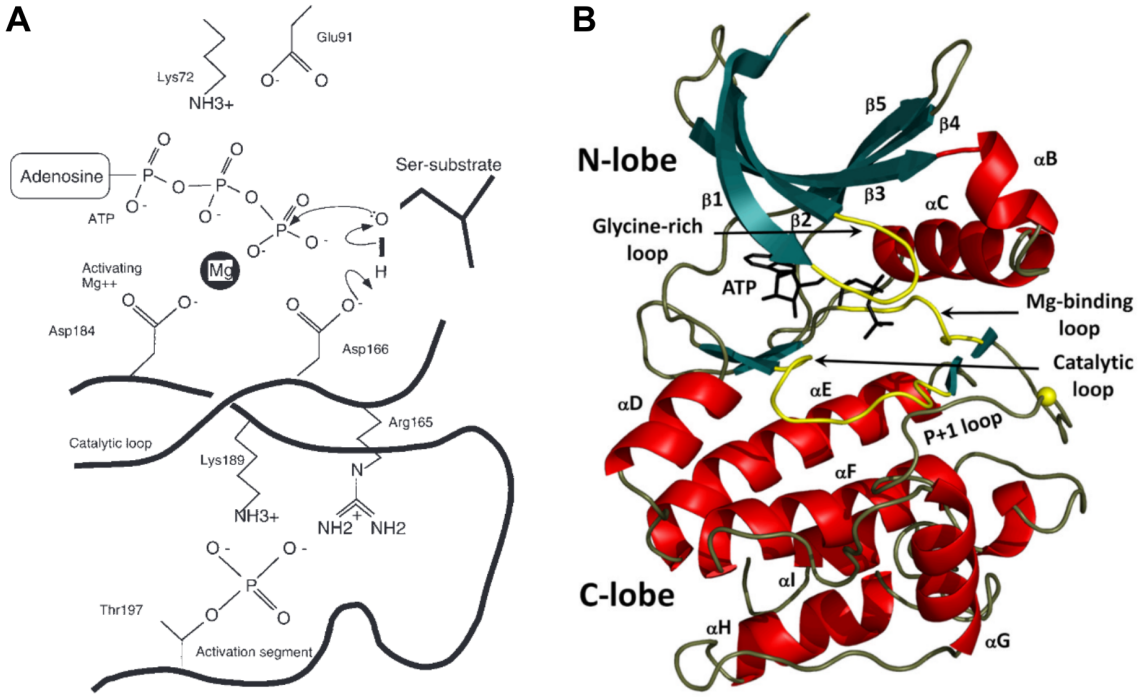

Figure 3. The protein kinase active site and mechanism of the phosphotranspherase reaction. ***A.*** *The assumed mechanism of the phosphotransferase reaction in the catalytic centre of the protein kinase A. The carboxylate of Asp166 activates the –OH group of the acceptor serine for the nucleophylic attack of the γ-phosphate of ATP.* ***B.*** *Structure of the conserved protein kinase core (structure from PKA). The N-terminal lobe consists of five β-sheets (turquoise) and conserved C-helix (red). The C-terminal lobe is mostly α-helical (red). An ATP molecule (black) binds to the cleft between the two lobes. The most important loops are in yellow. Adapted from [2], [12].*

[13, 2]

The large, mostly α-helical C-terminal lobe contains the catalytic residues and the binding site for the substrate. For protein kinase activity, the catalytic loop (between β-sheets 6 and 7, consisting of Arg165 to Asn171 in PKA) and the metal binding loop (between β-sheets 8 and 9) are most important. The assumed mechanism is that Asp166 abstracts the proton from the –OH group of the substrate, where Lys168 (conserved in Ser/Thr-specific protein kinases) neutralizes the negative charge of the γ-phosphate and stabilizes the intermediate state. The metal-binding loop contains a conserved D-F-G region able to bind two metal ions, where one of them functions as a ligand for ATP, and the second one binds with low affinity and has an inhibitory effect. [14, 2]

Protein kinases exist in two states, active and inactive. The structure of the active state is similar between the individual kinases, where the structure of the inactive state is more variable. In the active state, the N- and C-lobes are closely

packed together and the sites for binding ATP and substrate are accessible. The inactive state is characterized by the more open conformation of the two lobes, where the mechanisms of stabilization of the protein in the inactive state differ between the individual protein kinases (e.g., binding of inhibitors, regulatory subunits, or phosphorylation). [2]

1.1.2 Cyclin-dependent protein kinases

Cyclin-dependent kinases (CDKs) are serine/threonine protein kinases that need an interaction partner, called a cyclin, for their activation. Without cyclins, CDKs are inactive. When a cyclin binds to a CDK, an active binary complex is formed (Fig. 4). In the complex, CDK carries catalytic activity, and cyclin activates CDK and helps to determine substrate specifity. In addition to cyclin regulation, most CDKs are also activated by phosphorylation in the activation segment. [2]

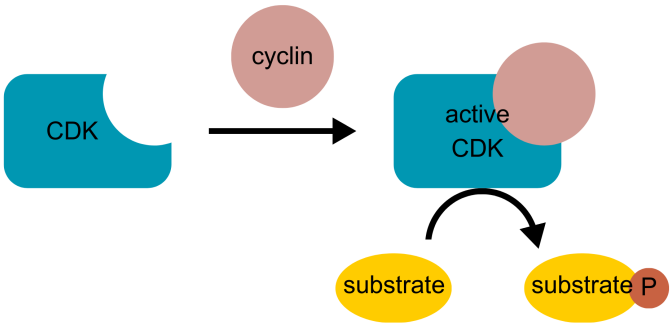

Figure 4. A scheme of CDK activation. *Without cyclins, CDKs are inactive. When a cyclin binds to a CDK, an active binary complex is formed. The cyclin-activated kinase is able to phosphorylate a substrate. Adapted from [15].*

There are 20 known CDKs differentiated into eight subfamilies (Fig. 5 on page 22) and 29 cyclins in human cells. CDKs from the CDK1, CDK4 and CDK5 subfamilies can be activated by multiple cyclins and play a role in the regulation of the cell cycle. According to Santamaría et al. [16], the only CDK necessary for the mammalian cell cycle is CDK1, where the others are dispensable and their functions can be taken over by CDK1. However, other cell-cycle CDKs also play an important role and are necessary under some specific conditions (e.g., growth after starvation). CDKs from the CDK7, CDK8, CDK9, CDK11, and CDK20 subfamilies can bind to only a single cyclin and function as transcription factors. The activity of CDKs during the cell cycle is regulated by cyclins and CDK inhibitors (CKIs). [4]

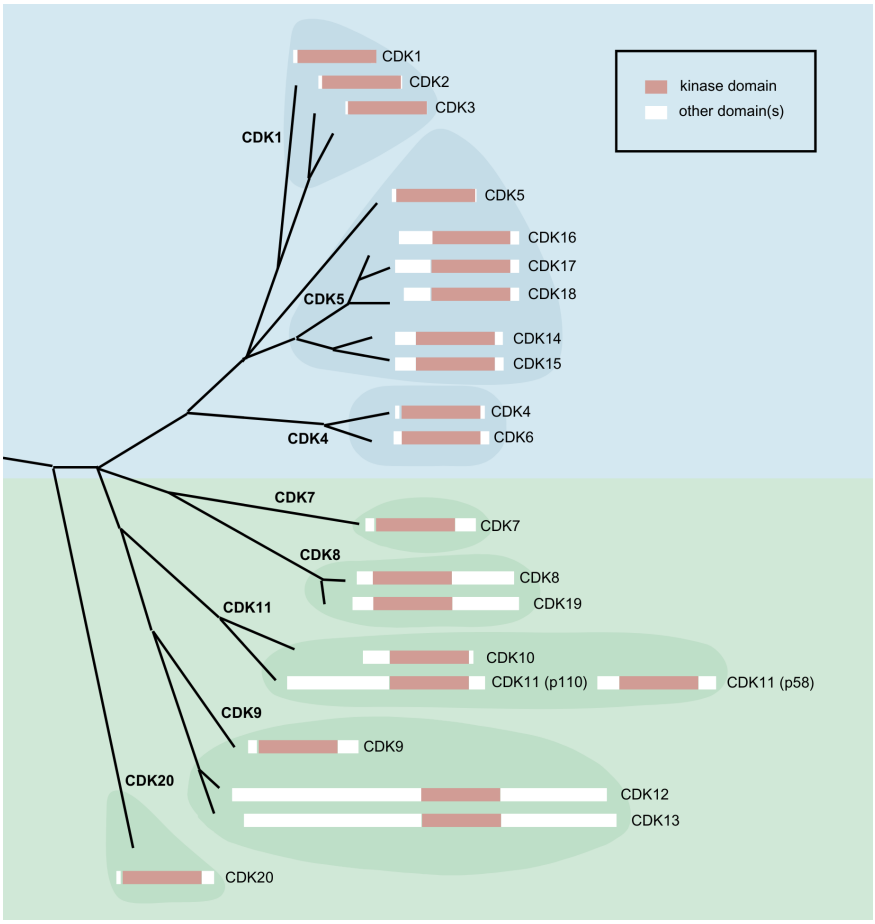

Figure 5. The evolution tree depicting the relations among the mammalian CDKs. *The upper (blue) part shows the cell-cycle connected CDKs, the bottom (green) part the transcriptional CDKs. The labels of the CDK subfamilies are in bold. All the CDKs share a conserved kinase domain (pink), but they differ in the length of their N- and C-terminal domains (white). The human CDK11 is present in two isoforms encoded by two separate genes, the longer ($CDK11^{p110}$) and shorter one ($CDK11^{p58}$). Adapted from [4].*

Cyclins

Cyclins are 35 to 90 kDa proteins that function mainly as allosteric activators of CDKs. They contain a single- or tandem-duplicated cyclin box domain (CBD) that mediates the interaction between cyclin and CDK. There are 46 known proteins containing CBD or CBD-like domains, 29 of which have been identified as direct activators of different CDKs. [2, 17]

The cyclin box domain is an approximately 100 amino acid long N-terminal fold formed by five α-helices. The second fold, present in the C-terminal part of all conventional cyclins, is necessary for the proper folding of the cyclin molecule and causes its rigid structure (cyclins hardly change their conformation while binding

CDKs). Its structure is highly similar to that of the N-terminal CBD, but its sequence is different. [18, 17, 19]

Cyclins are classified into three groups. Group I, which contains cyclins A, B, D, E, F, G, J, I, and O, plays the major role in the regulation of the cell-cycle CDKs. From group II, which contains cyclin Y and cyclin Y-like proteins, no member has yet been structurally characterized and its function must be further established. The members of group III, the cyclins C, H, K, L, and T, function as activators of transcriptional CDKs. [17, 4]

The levels of cyclins that bind to cell-cycle-related CDKs oscillate during the cell cycle and thereby cause the changing activity of CDKs during different cell-cycle phases (the periodically changing concentration also gave them the name "cyclins"). On the contrary, the cyclins that bind transcriptional CDKs do not show oscillating levels during the cell cycle. [4] The concentration of cyclins is regulated on the level of expression and targeted degradation (usually using the ubiquitine pathway), on the level of post-translational modifications mainly by phosphorylation at several sites, and also on the level of change in subcellular distribution. [2]

In addition to activating and contributing to CDK substrate specifity, some cyclins show other functions independent of CDK (for example, cyclin D1 is associated with transcription factors and other nuclear proteins). [2, 18] Some cyclins may even have the opposite function: e.g., cyclin E binds to CDK5 and inhibits its function. [17]

CDK inhibitors

CKIs are a heterogeneous group of proteins that can reversibly bind CDKs or CDK-cyclin complexes and inhibit their activity. They play the most important role in the transition between the G_1 and S phases and also in stopping the cell cycle and the transition to the G_0 phase. The question of whether CDKs are activated or inhibited is decided by the proportion between cyclins (activators) and CKIs (inhibitors). [20, 2]

1.1.3 Structure and regulation of CDKs

CDKs are members of the CMGC group of protein kinases and thus are proline-directed Ser/Thr-protein kinases. Having a hydrophobic pocket near the active site that binds to proline, their preferential phosphorylating motif is **S**/**T**-P-X-K/R (X is any residue). However, the K/R residue in the +3 position is not required for some (usually transcriptional) CDKs. Also, some CDKs are not proline-directed (CDK7, CDK9) and do not require proline in the +1 position.

The size of CDKs differs from the smallest CDKs, about 250 amino acids long,

containing only the kinase domain, to more than 1,500 residue-long proteins containing N and / or C-terminal domain(s) (Fig. 5 on page 22). The structure of the kinase domain corresponds to the conserved protein kinase structure (Section 1.1.1 on page 18) and consists of two lobes and the active site between them. [4] The N-terminal lobe consists of β-sheets and contains a glycine-rich inhibitory element (G-loop) and the C-helix (also known according to the sequence as PSTAIRE-helix) necessary for activation. The C-terminal lobe is mainly α-helical and contains the typical activation segment (T-loop) with phosphorylation-sensitive threonine. [2, 4]

In monomeric form without cyclin, the C-helix rotates so that conserved catalytic-active glutamate (Glu51 in CDK2) cannot interact with ATP-coordinating lysine (Lys33 in CDK2) at the active site. The active site is further blocked by the C-helix and the nonphosphorylated T-loop. When the cyclin binds to the C-helix, it rotates Glu to the active site and restores the ionic interaction of Glu and Lys. Thus, the active site is accessible for ATP binding and the kinase is activated (Fig. 6 on page 25). By phosphorylation of the active CDK-cyclin complex in the T-loop (Thr160 in CDK2), the active conformation is further stabilized. [21] On the other hand, phosphorylation of residues in the ATP-binding region (G-loop, Thr14 and Tyr15 in CDK2) leads to inhibition of CDKs. Through these variations of the processes, exact regulation of the activity of CDKs can be achieved. [2]

As the above-described mechanism can be applied to most CDKs, some exceptions are described. The active site of CDK4 is inaccessible for ATP after cyclin binding, although the mechanism of its activation is not yet completely clear. CDK5 does not require phosphorylation in the T-loop for activity. Furthermore, the N- and C- terminal extensions of CDK16, CDK17, and CDK18 play a non-negligible role in cyclin binding. [4]

1.2 Cyclin-dependent kinase 16

Cyclin-dependent protein kinase 16 (CDK16), also known as PCTAIRE-1 kinase (Fig. 7 on page 26), is a proline-directed Ser/Thr-protein kinase that binds to CCNY as its activator. It is a member of the PCTAIRE kinase group (together with its relatives CDK17 and CDK18), which members contain the substitution of cysteine for serine in C-helix binding to cyclins. CDK16 is highly conserved in the kinase domain and has both N- and C-terminal extensions that differ or are not present in other cyclin-dependent kinases.

CDK16 occurs exclusively in animals and is expressed in postmitotic cells. It is most abundant in the hippocampus and testis, although its transcripts and protein were detected in many other tissues. It functions mainly in neurons in the processes of intracelular vesicle formation and transport, participates in neurite outgrowth,

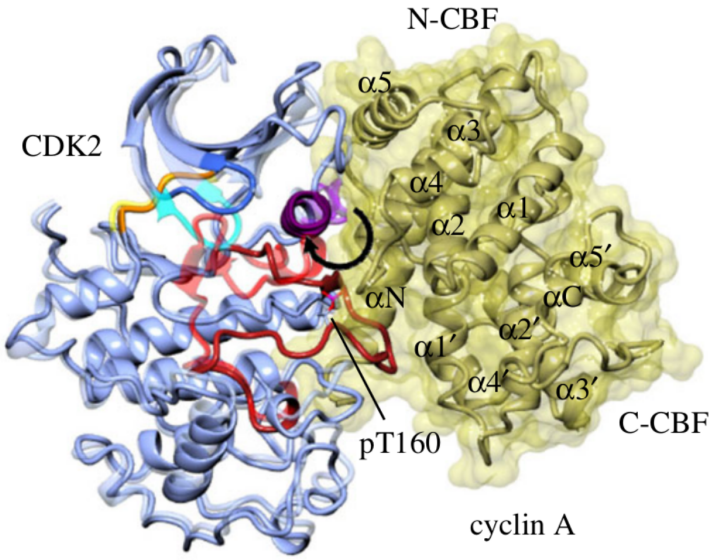

Figure 6. Activation of CDK2 by cyclin A (CCNA). *Overlay of monomeric CDK2 (transparent, blue) and Thr160-phosphorylated CDK2 (blue) in complex with CCNA (yellow). CCNA is composed of two cyclin box domains (N-terminal N-CBD and C-terminal C-CBD). While CDK2 binds CCNA, the C-helix (violet) rotates and enables the ionic interaction of Glu and Lys necessary for the catalytic activity. The activation loop (red) is extended and pulled away from the active site. CCNA binding changes the conformation of N- and C-terminal lobes and enables the propper orientation of the ATP and the substrate in the active site. The Thr160 phosphorylation stabilizes the active conformation of the complex. Retrieved from [22]*

and is essential for the differentiation of spermatozoa during spermatogenesis in testes. [18, 5, 24] According to Shetata et al. [25], CDK16 participates in vesicle trafficking and synaptic transmission by phosphorylating AP2-associated kinase 1 (AAK1), dynamin 1, and synaptojanin 1, which all play a key role in neuronal regulation. Through these interactions, CDK16 enables the axonal transport of presynaptic components and maintains the ballance between anterograde and retrograde transport. [26] CDK16 has also been found to play a role in the development of X-linked intellectual disability. [27, 5]

The subcellular location of CDK16 is predominantly the cytoplasm of neurons and nucleolus, whereas the CDK16–CCNY complex binds through the myristoylation of CCNY to the plasma membrane. [18] The level of CKD16 is stable during the cell cycle, unlike activity, which is lowest during the G_1 to S phase transition and reaches its maximum during the S and G_2 phase. During the cell cycle, CDK16 is actively transported out of the nucleus to the cytoplasm, indicating that CDK16 is not involved in DNA replication. [28]

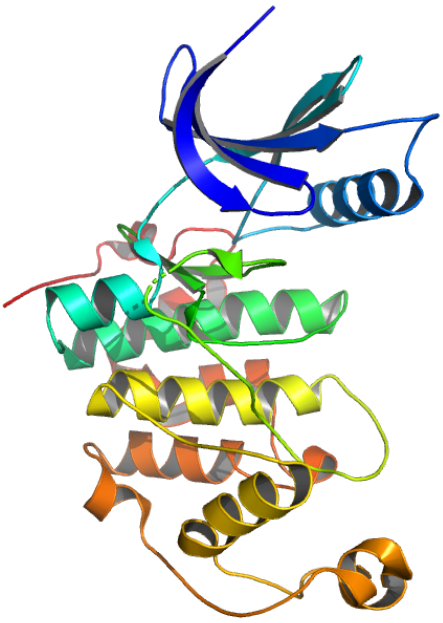

Figure 7. Crystal structure of human CDK16 with inhibitor (PDB ID: 5G6V). *The upper (blue) part is the N-terminal lobe consisting of five-stranded β-sheet and the C-helix. The multi-coloured C-terminal lobe is mostly α-helical. The picture was created in PyMOL. [23]*

1.2.1 Cyclin Y

CCNY, the allosteric binding partner and activator of CDK16, is highly conserved throughout the species over its entire length. Human CCNY is a 341 amino acid long protein that (unlike the other cyclins) has only the N-terminal, CDK-binding cyclin fold between residues 143–243. At both N- and C- termini, CCNY contains long extension domains. Except for CDK16, it binds and also activates the other PCTAIRE- and PFTAIRE-kinases (CDK14–18). [6, 29]

CCNY plays an important biological role: for many organisms, its absence during development is lethal and its mutations cause many developmental defects. [30] According to Li et al. [31], CCNY is also an oncoprotein that plays a role in the development, progression and metastasis of different types of cancer by regulating mitotic spindle formation. Thus, together with CDK16, CCNY is a potential novel therapeutic target for cancer therapy.

1.2.2 CDK16–CCNY interaction

For the creation of the active CDK16–CCNY complex, the previous interaction of CCNY with 14-3-3 proteins is necessary. In the interaction of CCNY with 14-3-3 proteins, both the N- and C-terminal domains are involved outside the cyclin box. [5, 29] In these regions, there are two phosphorylation sites, S100 and S326, which, when

phosphorylated, are binding sites for 14-3-3 proteins. When the sites are mutated or not phosphorylated, CCNY cannot bind to 14-3-3 proteins and therefore cannot bind and activate CDK16. [5]. This leads to the hypothesis that is further investigated in the experimental part of this thesis, that CDK16 is activated by a novel mechanism containing formation of the CDK16–CCNY–14-3-3 ternary complex.

1.3 14-3-3 proteins

The 14-3-3 proteins (Fig. 8) are a family of structurally similar acidic proteins (the pI of all isoforms is approximately 4.5). 14-3-3 proteins were first found and characterized in the brain [32] but are present in all types of eukaryotic cells. The name 14-3-3 comes from their specific migration pattern on 2D DEAE–cellulose chromatography and starch gel electrophoresis. [33, 34] There are seven 14-3-3 human isoforms: β/α, γ, ϵ, ζ/δ, η, τ and σ, where α and δ are one times phosphorylated forms of the isoforms β and ζ, respectively. [35, 36] Unicellular organisms (such as budding yeast) express only two 14-3-3 protein isoforms [37], when plants contain fifteen. [38]

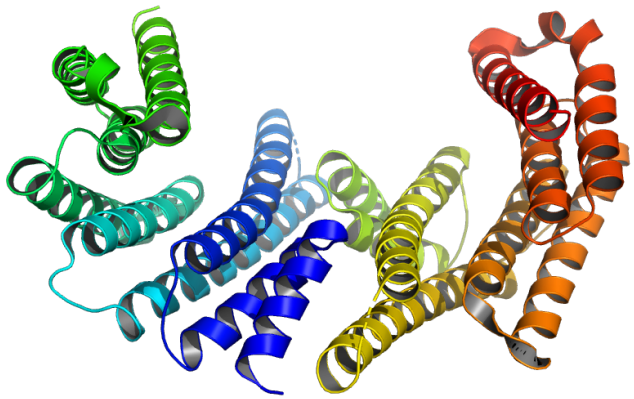

Figure 8. Crystal structure of human 14-3-3 γ with transcription factor EB 14-3-3 binding motif (PDB ID: 6A5S). *The picture was created in PyMOL. [39]*

14-3-3 proteins play an important role in many cellular processes: they influence the cell cycle, regulate apoptosis and autophagy [40] and play a role in the regulation of many protein kinases. In the RAS-RAF-MEK-ERK signaling pathway, they function as a key binding partner of RAF kinase, which helps to stabilize both the inactive and the active states of the kinase. [36, 41] 14-3-3 proteins also bind and inhibit apoptosis signal-regulating kinase 1 (ASK1) and calcium/calmodulin-dependent protein kinase kinases (CaMKK). [36] And, as discussed in Section 1.2.2 on page 26, 14-3-3 proteins also play an important role in the regulation and activation of CDK16, binding to its activation binding partner, CCNY.

1.3.1 Structure of 14-3-3 proteins

14-3-3 proteins form stable homo and heterodimers with monomers of size 30 kDa. Each monomer consists of 9 antiparalell α-helices (H1 to H9, Fig. 9), where the first four helices participate in dimer formation and the helices H3, H5, H7 and H9 form a ligand-binding groove consisting of basic residues on one side (R57, R130, and Y131 in 14-3-3 η) and hydrophobic residues on the other side. [42, 43]

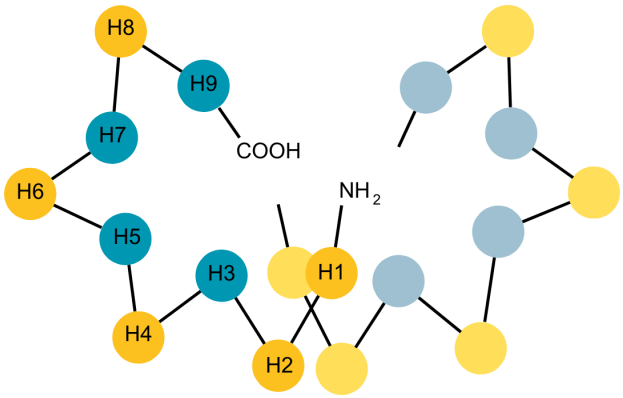

Figure 9. Schematic structure of the 14-3-3 dimer. *Each monomer consists of 9 α-helices H1 to H9. The helices H1 to H4 participate on the dimer formation and the helices H3, H5, H7 and H9 form a ligand-binding groove (blue). Outer helices are in yellow. Adapted from [42].*

For the dimerization of the 14-3-3 protomers, the formation of salt bridges at the interaction interface is crucial. In 14-3-3 ζ homodimer, helices H1 and H2 of one protomer interact with H3 and H4 of the other protomer through three salt bridges, where only one of them is conserved in all isoforms. The interaction is further stabilized by other hydrophobic and polar bonds. The ability to form the salt bridges predetermines the preference of individual isoforms for homo- or heterodimerization. The ϵ isoform at homodimeric state forms only one salt bridge, unlike three salt bridges in the heterodimeric state. Therefore, it is preferentially present in heterodimer. On the contrary, the σ isoform is present exclusively in the homodimeric state due to several unique interactions between the σ protomers. [44]

When dimerized, the 14-3-3 cup-like structure creates a large, negatively charged binding groove (approximately 3.5 nm broad, 3.5 nm wide and 2.0 nm deep). The inner surface of the binding groove mainly consists of invariant residues, where the variable residues are oriented mostly out of the groove. The flexible 15–40 amino acid long C-terminal loop shows high sequential variability across the isoforms. Due to its intrinsically disordered character, its structure remains unknown. When 14-3-3 is unbound, the C-terminal loop occupies the binding groove and disables unspecific interactions. During the formation of a specific interaction between 14-3-3 and its

ligand, the C-terminal loop is displaced from the binding groove. [44, 45]

Although highly conserved, individual 14-3-3 isoforms differ in the angle between the two subunits that is caused by small structural alterations. This enables binding ligands of different sizes and shapes into the binding groove of individual dimers. Further structural variations occur in the length and conformations of the loop regions connecting individual helices (especially between H3/H4 and H8/H9) and in the length of the helices H3 and H4. [44, 46]

1.3.2 Formation of complexes with 14-3-3 proteins

The 14-3-3 proteins usually interact with their binding partners as dimers, although under specific conditions they can also bind in the monomeric state [43]. Due to the strong bonds between individual helices in their structure, 14-3-3 proteins are rigid molecules that can function as platforms for the reshaping of bound proteins. There are three known motifs for 14-3-3 binding, where motifs I and II with sequence R-(X)-[S/Φ]-[+]-pS-X-P (where X is any residue, Φ is aromatic residue and + is basic residue; motifs I and II differ in the presence or absence of (X)) are significantly stronger than motif III with sequence pS/pT-X-(X)–COOH (presence of (X) is optional). Still, other binding motifs exist, containing phosphothreonine instead of phosphoserine or even non-phosphorylated. [47, 44]

In the 14-3-3 dimers, the protomers are bound together in an antiparallel manner. This property enables usage of the binding grooves of both protomers by the substrates containing more than one 14-3-3 binding motifs. [44] According to Kostelecky et al. [48], ligands with two 14-3-3 binding sites that are at least ten residues away bind with significantly higher affinity. Binding with two different sites is also probably necessary for the full biological activation of the complex. The 14-3-3 binding motifs are usually located in the disordered regions of the target proteins. Probably, the higher flexibility of disordered regions makes them more universal and easily regulated and enables them wider radius when looking for the binding partner. [44]

14-3-3 proteins participate in many biological processes and have variety of functions based on different mechanisms. By interacting with target proteins, they mediate three different types of actions (Fig. 10 on page 30):

1. Directed conformational changes of target proteins. Due to interaction with 14-3-3 proteins, the target proteins can be activated by stabilizing its active conformation or inactivated by changing the conformation of the active site.

2. Physical occlusion of sequence-specific or structural features. Binding to 14-3-3 proteins through sequences near the active site or important structural features masks these parts of the protein and disables other interactions with the 14-3-3-bound protein. 14-3-3 protein masking can also protect phosphorylated

proteins from dephosphorylation by preventing phosphatases from accessing the phosphorylated residues. The binding of 14-3-3 proteins can also change the subcellular location of the target protein.

3. Scaffold mediating protein-protein interactions. When two different proteins bind to the same 14-3-3 protein dimer, their close proximity and restricted orientation allow for specific regulation and targeting of protein-protein interactions (e.g., phosphorylation). [49, 44]

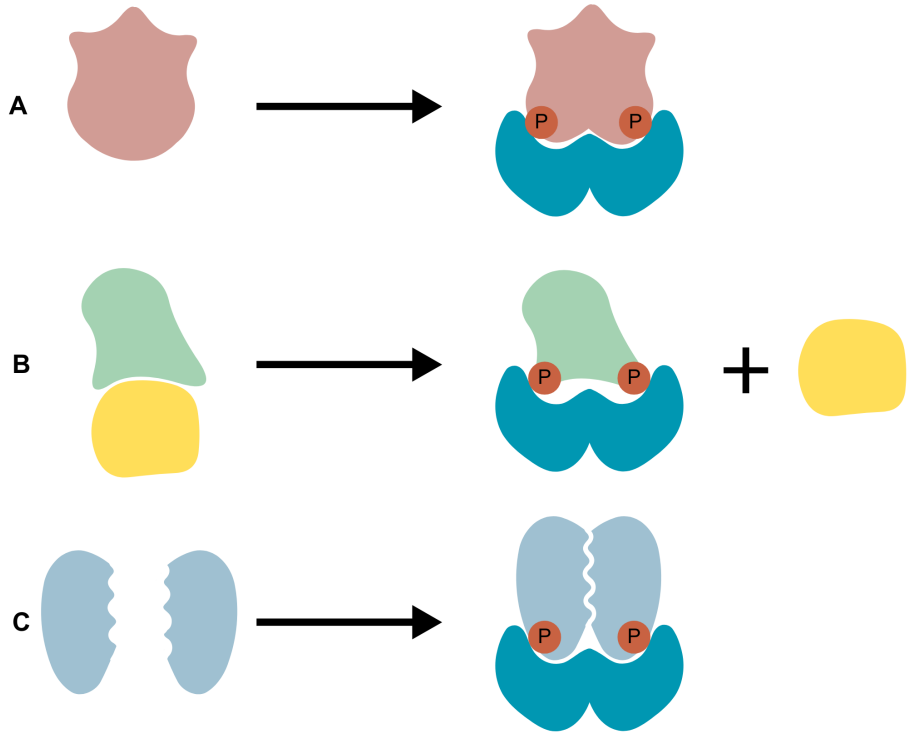

Figure 10. 14-3-3 proteins mediate three different types of actions. ***A.*** *Directed conformational changes of target proteins.* ***B.*** *Physical occlusion of sequence-specific or structural features.* ***C.*** *Scaffolding mediating the protein-protein interactions. Adapted from [49].*

1.3.3 Regulation of 14-3-3 proteins

14-3-3s are important regulatory proteins and are also regulated by several mechanisms. 14-3-3 proteins are expressed in all tissues, except of the mammalian σ isoform that is more tissue-specific. Post-translationally, 14-3-3 proteins are regulated by phosphorylation at several sites that are not conserved across the isoforms (S58, S184, and S233 in 14-3-3 ζ). Therefore, the heterodimerization and isoform specifity may play an important role. Furthermore, 14-3-3 proteins can also be regulated by cofactors, e.g., AMP or magnesium. [50, 51, 49]

Aims of the thesis

1. Comparison of binding affinities of all human 14-3-3 isoforms for 14-3-3 binding motifs of human CCNY using fluorescence anisotropy measurements.
2. Expression and purification of selected 14-3-3 isoforms, CCNY and CDK16.
3. Phosphorylation of CCNY.
4. Characterization of the pCCNY–14-3-3 interaction by native electrophoresis.
5. Characterization of the pCCNY–14-3-3 γ and CDK16–pCCNY–14-3-3 γ complexes using size exclusion chromatography.
6. Refinement of the crystal structure of the 14-3-3-binding motif `RKRSApSADNL` of CCNY bound to 14-3-3 γ.

Chapter 2

Materials and Methods

2.1 Materials

2.1.1 Biological materials

BSA ..... Sigma-Aldrich, USA
DNase I ..... ZellBio, Germany
Escherichia coli BL21(DE3) strain ..... Stratagene, USA
Escherichia coli BL21(DE3)RIPL strain ..... Stratagene, USA
Lysozyme ..... SERVA Electrophoresis, Germany
Peptide CCNY_pS100 (Tab. A.1 on page 83) ..... Pepscan, Netherlands
Peptide CCNY_pS326 (Tab. A.2 on page 83) ..... Pepscan, Netherlands
Peptide FLC-CCNY_S100 (Tab. A.3 on page 83) ..... Pepscan, Netherlands
PKA ..... prepared in our laboratory
PreScission Protease ..... prepared in our laboratory
Roti Mark Tricolor protein marker ..... Carl Roth, Germany
TEV protease ..... prepared in our laboratory

2.1.2 Chemicals

1,4-dithiothreitol ..... Carl Roth, Germany
β-mercaptoethanol ..... Sigma-Aldrich, USA
HEPES ..... Sigma-Aldrich, USA

Acrylamide ..... Carl Roth, Germany
ADP-Glo™ Kinase Assay ..... Promega, USA
APS ..... Sigma-Aldrich, USA
Ampicillin ..... Sigma-Aldrich, USA
ATP ..... Sigma-Aldrich, USA
Bis-acrylamide ..... Carl Roth, Germany
Bromophenol blue ..... Carl Roth, Germany
Calcium chloride ..... Penta, Czech Republic
Calibration buffers (pH = 4.01, 7.01) ..... Hanna Instruments, Czech Republic
Chloramphenicol ..... Sigma-Aldrich, USA
Coomassie Brilliant Blue R 250 ..... LKB Bromma, Sweden
Disodium hydrogen phosphate dodecahydrate ..... Penta, Czech Republic
EDTA ..... Lachema, Czech Republic
Electrophoresis Loading-Dye ..... New England BioLabs, USA
Ethanol 96% ..... Lach-Ner, Czech Republic
Glutathione reduced ..... Sigma-Aldrich, USA
Glycerol ..... Penta, Czech Republic
Guanidine hydrochloride ..... Sigma-Aldrich, USA
Hydrochloric acid ..... Penta, Czech Republic
Imidazole ..... Carl Roth, Germany
IPTG ..... EMD Biosciences, Germany
Isopropanol ..... Genomed, Germany
LB medium ..... Carl Roth, Germany
Magnesium chloride ..... Lach-Ner, Czech Republic
Methanol ..... Lachema, Czech Republic
Nickel sulfate hexahydrate ..... Penta, Czech Republic
PMSF ..... Carl Roth, Germany
Potassium phosphate monobasic ..... Sigma-Aldrich, USA
Rotiphorese gel ..... Carl Roth, Germany
Sodium azide ..... Sigma-Aldrich, USA
Sodium chloride ..... Lach-Ner, Czech Republic
Sodium dihydrogen phosphate dihydrate ..... Penta, Czech Republic
SDS ..... Carl Roth, Germany
Sodium hydroxide ..... Lach-Ner, Czech Republic

TCEP ..... Sigma-Aldrich, USA
TEMED ..... Carl Roth, Germany
Tris ..... Carl Roth, Germany
Tween ..... Carl Roth, Germany

2.1.3 Instruments

3505 pH Meter ..... Nova Capital, United kingdom
Analytical scales EG420-3NM ..... Kern, Germany
Automatic pipettes ..... Eppendorf, Germany
Centrifuge 5804R (rotor A-4-44) ..... Eppendorf, Germany
Centrifuge Hermle Z323K ..... Hermle, Germany
Centrifuge MiniSpin PL-109 ..... Eppendorf, Germany
Centrifuge Sigma 8K (rotor 12510-H) ..... Sigma, Germany
CLARIOstar microplate reader ..... BMG Labtech, Germany
FPLC ..... Watrex Praha, Czech Republic
FPLC AKTA ..... GE Healthcare, USA
Gallenkamp Orbital Incubator shaker ..... Gemini BV, Netherlands
Laboratory scales EG-420 NM ..... Kern, USA
Magnetic stirrer Variomag Maxi, Komet ..... Thermo Scientific, USA
NanoDrop One ..... Thermo scientific, USA
Peristaltic pump Ecoline ..... Ismatec, Germany
Shaker Multitron Infors ..... AG, Switzerland
Shaking incubator NB-205 ..... N-BIOTEK, Republic of Korea
Sonicator 3000 ..... Misonix, USA
Source for vertical electrophoresis ..... Bio-Rad Laboratories, USA
Spectrophotometer IMPLEN P300 ..... BioTech, USA
Spectrophotometer NanoDrop ..... Thermo Fisher Scientific, USA
Thermal block ..... Grant, UK
Vertical electrophoresis ..... Bio-Rad Laboratories, USA
Vortex ZX3 ..... VELP Scientifica, Italy

2.1.4 Other materials

Amicon Ultra concentrators ..... EMD Millipore, USA
Automatic pipette tips ..... Axygen, USA
Centrifuge cuvettes ..... Carl Roth, Germany
Chelating Sepharose Fast Flow ..... GE Healthcare, USA
Dialysis membrane, type 27/32 ..... Carl Roth, Germany
Flat bottom 384-well plate black color ..... Corning, USA
Flat bottom 384-well plate white color ..... Greiner Bio-One, Austria
Conical bottom 96-well plate white color ..... Roche Diagnostics, Switzerland
Glutathione Sepharose 4 Fast Flow ..... GE Healthcare, USA
HiTrap Q sepharose ..... GE Healthcare, USA
Laboratory glass ..... Simax, Czech Republic
Microtubes ..... P-LAB, Czech Republic
Nickel chelating chromatography column ..... Bio-Rad Laboratories, USA
Spartan 13/0.45 RC filter unit ..... GE Healthcare, USA
Superdex 75 HiLoad 26/600 column ..... GE Healthcare, USA
Superdex 200 HiLoad 26/600 column ..... GE Healthcare, USA
Superdex 200 Increase 10/300 column ..... GE Healthcare, USA
Syringes ..... Braun, Germany
Test tubes ..... Thermo Fisher Scientific, USA
Vivaspin Turbo centrifugal filter device ..... Sartorius, United kingdom
Whatman^{TM} membrane filter paper 0.45μmol dm^{-3} ..... GE Healthcare, USA

2.2 Methods

2.2.1 Fluorescence anisotropy

The fluorescence anisotropy assay is based on irradiation of fluorophore-labeled samples by plane-polarized light and the recording of the light emitted by the fluorophore. In a solution, the light will preferably be absorbed by the molecules whose absorption oscillators are parallel to the plane of polarized light. When the molecules do not change their spatial orientation, the light emitted by the fluorophore is also plane-polarized. The fluorescence anisotropy in the sample is described by the Perrin

equation:

$$\frac{1}{r} = \frac{1}{r_0} + \left(\frac{1}{r_0} - \frac{1}{3}\right) \cdot \frac{RT}{V} \cdot \frac{\tau}{\eta}, \tag{2.1}$$

where r is the anisotropy, r_0 is the maximum anisotropy, R is the gas constant, T is the temperature, V is the molar volume of the fluorescent substance, τ is the average lifetime of the excited state of fluorophore and η is the viscosity.

In the solution, the molecules constantly change spatial orientations. The rate of these movements depends on the rotational relaxation time ϕ according to the equation 2.2:

$$\phi = 3\eta \cdot \frac{V}{R} \cdot T, \tag{2.2}$$

where η is the medium viscosity, V is the molecular volume, R is the gas constant and T is the temperature.

Therefore, under constant temperature and viscosity of the solution, the fluorescence anisotropy is directly proportional to the molecular volume. Large molecules hardly change their orientations between absorbtion and emission. On the contrary, small molecules move very quickly and can assume any orientation between the absorbtion and emission. Therefore, fluorescence of large molecules is highly polarized, while fluorescence of small molecules is almost completely depolarized. This phenomenon is expressed by fluorescence anisotropy r:

$$r = \frac{I_{||} - I_{\perp}}{I_{||} + 2I_{\perp}}, \tag{2.3}$$

where $I_{||}$ is the vertical component of fluorescence and $I_{\perp}$ is the horizontal component. By fluorescence anisotropy, the changes of the volume of the molecules can be measured. The changes of the molecular volume can be caused by creation or dissociation of the molecular complexes, binding of ligands or through conformational changes of the molecules [52, 53].

The fluorescence anisotropy assay used in this work is based on mixing the fluorophore-labeled peptide with the unlabeled 14-3-3 protein molecule. When the peptide stays unbound in the sample, the measured fluorescence anisotropy is minimal because of the fast movement of the small molecule in the solution. On the contrary, the 14-3-3 protein bound peptide is a relatively large structure that changes orientation much slower and the fluorescence anisotropy decreases slowly. The structure of the peptides used structurally responded to the 14-3-3 protein binding sites of the CCNY molecule. Using this assay, the affinity of particular 14-3-3 protein binding sites of the CCNY can be measured for different isoforms of the 14-3-3 protein.

The affinity of all 14-3-3 protein isoforms was measured for three different peptides. The CCNY_pS100 (parameters in Tab. A.1 on page 83) and CCNY_pS326 (parameters in Tab. A.2 on page 83) peptides were mimicking the phosphorylated

14-3-3 protein binding sites of CCNY (S100 and S326, respectively), where the FLC-CCNY_S100 peptide (parameters in Tab. A.3 on page 83) was mimicking the unphosphorylated CCNY site S100.

The 14-3-3 protein isoforms (β, γ, δ, ϵ, ζ, η, τ) were dialyzed to 1× HBS buffer (Tab. VI) at 4 °C overnight. The next day, the samples for the fluorescence polarization assay were prepared in the black 384-well plate (one plate was used for each peptide). The setup of each plate was following:

- first row: 20 μl of 50 nM peptide with 0.1% tween, 0.1% BSA and 1mM TCEP in each well,
- second row: 20 μl of 1× HBS (Tab. VI) with 0.1% tween, 0.1% BSA and 1mM TCEP in each well,
- the next rows: series of dilution of 50 nM peptide and 80 to $1 \cdot 10^{-3}\mu$M 14-3-3 protein isoform in 1× HBS (Tab. VI) with 0.1% tween, 0.1% BSA and 1mM TCEP,

where each isoform was prepared in triplicates. The plate was centrifuged at room temperature for 5 min at 58 g and allowed 60 min to incubate in the dark. Then, the fluorescence anisotropy was measured using the ClarioStar program.

Table VI. 10× HBS buffer

Buffer contents	
HEPES pH 7.4	0.1 mol dm^{-3}
NaCl	1.5 mol dm^{-3}

2.2.2 Expression and purification of 14-3-3 eta and gamma

Expression

The full-length human wild type 14-3-3 η (sequence in Tab. A.4 and Tab. A.5, parameters in the Tab. A.6, all on page 84) and 14-3-3 γ (sequence in Tab. A.7 on page 84 and Tab. A.8, parameters in the Tab. A.9, both on page 85) with N-terminal fusion Histag anchors were expressed in *E. coli* BL21(DE3) cells with pET-15b plasmid. Three 5ml cultures of sterile LB medium (Tab. A.16 on page 88) containing 100 μg/ml of ampicillin were inoculated with *E. coli* cells from the glycerol stock (containing 700 μl of the cell suspension and 300 μl of sterile glycerol) and incubated overnight at 37 °C and 180 rpm. The pET-15b plasmid contains a resistance gene against ampicillin. Therefore, only the cells containing the plasmid grow in the ampicillin-containing medium.

The next day, the overnight cultures were used as starting cultures. Each test tube was added to 1 liter sterile LB medium containing 100 μg/ml ampicillin and grown at 37 °C and 190 rpm. Every hour, the optical density at wavelength 600 nm (OD_{600}) of the culture was measured using pure LB medium as a blank. When OD_{600} reached 0.8 cm^{-1}, protein expression was induced using 1 ml of 0.5mol dm^{-3} IPTG.

The 14-3-3 η gene is cloned in the pET-15b plasmid under the *lac* operone, whose transcription is blocked by the *lac* represor. IPTG structure is similar to the structure of allolactose, a lactose metabolite that binds to and releases the *lac* represor and enables *lac* operone transcription.

After IPTG induction, the culture was incubated at 30 °C overnight. The next day, the grown cultures were centrifuged 20 minutes at 2.073 g and the pellets were resuspended in 100 ml 2× lysis buffer (Tab. VII). The resuspended cells were frozen at − 80 °C.

Table VII. 14-3-3 protein lysis buffer

Buffer contents	
PBS (Tab. A.17 on page 88)	1×
NaCl	1 mol dm^{-3}
β-mercaptoethanol	4 mmol dm^{-3}
imidazole	2 mmol dm^{-3}

Cell lysis

Next day, the cells were thawed and incubated with lysozyme (100 μg/ml) for 20 min at 4 °C by continuous stirring. The lysozyme hydrolyzes the polysacharide chains of the bacterial cellular wall and helps to release the cellular content to the solution. Cell lysis and protein release were completed using ultrasound. Cells were sonicated (10 s on, 30 s off, 20 min total) and unwanted solid parts were centrifuged at 23.000 g for 45 min. During sonication, the bacterial culture was cooled in an ice bath to prevent ultrasound-induced heating. The supernatant containing the released 14-3-3 protein was further purified by nickel chelating chromatography.

Nickel chelating chromatography

The used 14-3-3 η and 14-3-3 γ constructs contain a polyhistidine tag that allow purification using nickel chelating chromatography. The purification column contains the solid support, spacer arms, and, in particular, chelators that immobilize Ni^{2+} ions. During purification, histidine electron donor groups coordinate the Ni^{2+} ions in the column. Therefore, the recombinant protein containing the polyhistidine fusion tag binds to the column where the other proteins and molecules run through.

For the elution of the bound protein, the ligand exchange or deprotonation of the imidazole group of histidine can be used by lowering the pH [54]. In our protocol, a high concentration of imidazole is used in the elution buffer. Imidazole in the elution buffer competes with the histidines of the His-tagged protein for binding to Ni^{2+} ions in the column and allows the release of the protein from the column.

At first, a column for nickel chelating chromatography was prepared. The 5 ml of the chelating sepharose in the plastic column was washed with 20 ml water, 20 ml of 0.1 mol dm^{-3} Ni^{2+}, 20 ml water and 15 ml of starting buffer (Tab. VIII). The sonicate was then adsorbed on the column and washed with 300 ml of 10% elution buffer (Tab. IX) in starting buffer to elute all unbound or poorly bound molecules.

Table VIII. Starting buffer

Buffer contents	
PBS	1×
NaCl	0.5 mol dm^{-3}
β-mercaptoethanol	2 mmol dm^{-3}
imidazole	1 mmol dm^{-3}

Table IX. Elution buffer

Buffer contents	
PBS	1×
NaCl	0.5 mol dm^{-3}
β-mercaptoethanol	2 mmol dm^{-3}
imidazole	0.6 mol dm^{-3}

The fusion protein was eluted without pump with 20 ml elution buffer (Tab. IX) containing high concentration of imidazole. During the elution, 12 fractions were collected. The presence of 14-3-3 protein was confirmed using SDS PAGE.

SDS electrophoresis

For the confirmation of the presence and purity of the purified 14-3-3 protein, SDS PAGE (sodium dodecyle sulfate polyacryl amide gel electrophoresis) was used. 3 μl of each fraction was mixed with 2 μl of the sampling buffer (Tab. A.18 on page 89) and heated at 95 °C for 5 min. During heating, the protein strains are denatured and, due to the presence of β-mercaptoethanol in the sampling buffer, all disulfide bonds of the tertiary structure are reduced. The denatured proteins unfold into a rod-shaped structure with a series of negatively charged SDS molecules along the polypeptide chain (on average, one SDS molecule binds to every two amino acid residues). Therefore, the original native charge on the molecule is completely swamped by negatively

charged SDS molecules. The resulting negative charge depends only on the length of the polypeptide chain (a greater protein binds more SDS molecules and becomes more negatively charged). [55]

5 μl of the denatured samples were loaded onto the 15% polyacrylamide gel (contents in Tab. A.19, on page 89). In the first well, 3 μl of the protein standard was loaded. Electrophoresis was performed for 1 h at 200 V in 1× SDS buffer (Tab. X). In the electric field, denatured and SDS charged proteins move through the gel with a velocity that depends on their size (larger proteins have stronger negative charges and move faster).

Table X. 10× SDS PAGE buffer. *Contents for 1 liter.*

Buffer contents	
Tris	30 g
Glycine	144 g
SDS	10 g
H_2O	to 1 liter

The resulting gel was boiled in destiled water to fix the proteins in the gel and then stained with staining dye (Tab. A.23 on page 90) and heating. The stained gel was boiled in destiled water to remove the unbound dye and the presence and purity of the 14-3-3 protein in the individual fractions were confirmed. Fractions containing higher amounts of 14-3-3 protein were mixed and used for the next purification steps.

Dialysis and TEV cleavage

After elution, the sample contains a high concentration of imidazole that can interfere with protein concentration measurement (since imidazole absorbs UV rays in 280 nm) and could promote protein precipitation. Therefore, the mixed sample was dialyzed 2 h at 4 °C in dialysis buffer (Tab. XI) to lower the imidazole concentration.

Table XI. Dialysis buffer

Buffer contents	
Tris-HCl pH 7.5	20 mmol dm^{-3}
EDTA	2 mmol dm^{-3}
β-mercaptoethanol	2 mmol dm^{-3}
Glycerol	10%

In the fusion protein sequence, there is a TEV cleavage site between the N-terminal Histag and the target protein. This setting enables removal of the Histag after nickel-chelating chromatography. After dialysis, Histag was cleaved by TEV protease (250 U of TEV / 1 mg protein). The sample with TEV was incubated for 2 h at 30 °C and then dialyzed in dialysis buffer (Tab. XI) at 4 °C overnight.

Anion exchange chromatography

After dialysis, the TEV was removed using anion exchange chromatography with a Mono Q column using the flow rate 1 ml/min. The column contains the quarternary ammonium functional groups bound to the inertial matrix. The quarternary ammonium groups are positively charged, which enables the creation of ionic interactions between the column and negatively charged proteins. The strength of the interactions depends on the size of the negative protein charge, pH, and the ionic strength of the purification buffer used. [56]

14-3-3 proteins are acidic, with a pI of around 4.8. On the contrary, TEV is rather basic with pI around 8.9. At pH 8, the acidic 14-3-3 protein is significantly negatively charged where TEV is mostly uncharged. During purification using the Mono Q column, the 14-3-3 protein binds to the positively charged resin, and the TEV flows through.

The elution is performed by increasing the ionic strength of the buffer. Negatively charged ions in the buffer compete with the negative charge of the protein and, therefore, weaken the interaction between the protein and the column. [56] TEV, which is not bound to the column, elutes at a lower ionic strength, where 14-3-3 protein elutes at a higher ionic strength.

At first, the column was washed with 100% elution buffer (Tab. XII). Elution buffer contains a high concentration of sodium chloride, which effectively decreases the strength of the ionic bonds. The washing by elution buffer clears the column of all bound molecules from previous purifications. The column was then equilibrated with the starting buffer (Tab. XIII) until conductivity reached $3\,\mathrm{mS\,cm^{-1}}$. The sample was then loaded using FPLC at flow rate 1 ml/min.

Table XII. Elution buffer

Buffer contents	
Tris-HCl pH 8	$50\,\mathrm{mmol\,dm^{-3}}$
DTT	$1\,\mathrm{mmol\,dm^{-3}}$
NaCl	$1\,\mathrm{mol\,dm^{-3}}$

Table XIII. Starting buffer

Buffer contents	
Tris-HCl pH 8	$50\,\mathrm{mmol\,dm^{-3}}$
DTT	$1\,\mathrm{mmol\,dm^{-3}}$

14-3-3 protein was eluted using an increasing concentration gradient of NaCl. The applied gradient was the elution buffer 0 – 100 % in the starting buffer in 20 ml (flow

rate 1 ml/min). During purification, fractions containing the protein were collected and used for the next purification step.

Size exclusion chromatography

For the final removal of the contaminating proteins and 14-3-3 protein aggregates, size exclusion chromatography was performed using the Superdex 75 HiLoad 26/600 column. The column consists of dextrane covalently bound to cross-linked agarose, which creates pores of defined size. Proteins with hydrodynamic radius greater than that of the pores go through the column fast, without diffusion into the pores. Smaller proteins diffuse through the pores and are slowed down by the column. The protein sample loaded on the column is therefore divided by the size of the individual molecules [57].

For size exclusion chromatography, size exclusion buffer (Tab. XIV) and FPLC with flow rate 2 ml/min were used. Fractions were collected during purification and the presence and purity of the protein was confirmed using SDS PAGE. Into 5μl samples from each fraction, 3 μl of the sampling buffer (Tab. A.18 on page 89) were added, the samples were heated for 5 min at 95 °C and 5 μl was loaded on the polyacrylamide gel (Tab. A.19 on page 89) SDS PAGE was performed for 1 h at 200 V in 1× SDS buffer (Tab. X on page 41) and the resulting gel was stained with the staining dye (Tab. A.23 on page 90). In the end, the fractions containing protein were mixed and the concentration was measured.

Table XIV. Buffer for size exclusion chromatography

Buffer contents	
Tris-HCl pH 7.5	50 mmol dm^{-3}
NaCl	150 mmol dm^{-3}
EDTA	1 mmol dm^{-3}
DTT	5 mmol dm^{-3}
glycerol	10 %

Concentration and yield determination

After size exclusion chromatography, the concentration of the resulting protein was measured at 280 nm using NanoDrop. From the average of three measured values, the concentration was calculated using the equation

$$c = \frac{A_{280}}{\epsilon_{280} \cdot l}, \tag{2.4}$$

where A_{280} is absorbance at 280 nm, ϵ_{280} is molar absorbtion coefficient at 280 nm in mol^{-1} dm^3 cm^{-1} (for 14-3-3 η in Tab. A.6 on page 84, for 14-3-3 γ in Tab. A.9 on

page 85) and l is optical path length in cm.

The yield was calculated using the equation

$$m = c \cdot M \cdot V, \tag{2.5}$$

where c is the protein concentration in $\mathrm{mol\,dm^{-3}}$ (calculated using Eq. 2.4 on page 43), M is the molar mass of the protein in $\mathrm{g\,mol^{-1}}$ (for 14-3-3 η in Tab. A.6 on page 84, for 14-3-3 γ in Tab. A.9 on page 85) and V is the volume of the sample in $\mathrm{dm^3}$.

The protein aliquots were stored at − 80 °C.

2.2.3 Expression and purification of CCNY

Expression

The human CCNY (1–341 with mutations Y98R, S99A, S324A) with the N-terminal glutathion S-transferase (GST) fusion anchor (sequence in Tab. A.10 on page 85 and Tab. A.11, parameters in the Tab. A.12, both on page 86) was expressed in *E. coli* BL21(DE3)-RIPL cells containing pGEX-6P-1 plasmid. Initially, six starting cultures were prepared by mixing 5 ml of sterile LB medium with ampicillin and chloramphenicol to final concentrations of 100 μg/ml. Ampicillin ensures the growth of only cells with the pGEX-6P-1 plasmid. Chloramphenicol resistance is special for BL21(DE3)-RIPL cells and ensures the transcription of additional tRNA (argU (AGA, AGG), ileY (AUA), proL (CCC), and leuW (CUA) codons) in two additional plasmids. Cultures were inoculated by *E. coli* cells from the glycerol stock (700 μl of cell suspension, 300 μl of sterile glycerol) and incubated overnight at 37 °C, 180 rpm.

The next day, each starting culture was mixed with 1 liter of sterile LB medium containing 100 μg/ml of ampicillin and 100 μg/ml of chloramphenicol and grown at 37 °C, 190 rpm. Every hour, the $\mathrm{OD_{600}}$ of the suspension was measured using pure LB medium as a blank. When $\mathrm{OD_{600}}$ reached $0.8\,\mathrm{cm^{-1}}$, the temperature was lowered to 15 °C to preserve the protein that will be produced. Protein production was induced using 1 ml of $0.5\,\mathrm{mol\,dm^{-3}}$ IPTG and the cultures were incubated at 15 °C, 190 rpm overnight.

Cultures grown were centrifuged 20 minutes at 2.073 g and pellets were resuspended in 180 ml lysis buffer (Tab. XV). Resuspended cells were frozen at − 80 °C.

Table XV. Lysis buffer

Buffer contents	
PBS	2×
EDTA	$1\,\mathrm{mmol\,dm^{-3}}$
DTT	$10\,\mathrm{mmol\,dm^{-3}}$
$\mathrm{MgCl_2}$	$2\,\mathrm{mmol\,dm^{-3}}$

Cell lysis

Next day, the cells were thawed and incubated with lysozyme (100 μg/ml) and DNase I (250 μl per 100 ml of lysate) for 40 min at 4 °C. The lysozyme hydrolyzes the cellular wall and helps to release the protein where DNase degrades the cellular DNA and prevents clogging of the purification column. Then phenylmethylsulfonyl fluoride (PMSF) was added (1 ml PMSF per 100 ml lysate) to inhibit serine proteases that may cause degradation of the expressed protein.

The cells were then sonicated (10 s on, 30 s off, 18 min total) in an ice and water bath and the sonicate was centrifuged at 23.000 g for 45 min. A supernatant with the released recombinant protein was used for further purification.

GST chromatography

CCNY is expressed as a fusion protein containing the N-terminal GST tag that is used for purification and improves the solubility of the protein. The natural substrate of glutathione-S-transferase is a reduced glutathion that is immobilized in the glutathione sepharose column. When centrifuged sonicate is mixed with glutathione sepharose, the GST-CCNY protein binds to the slurry and can be easily separated from the other molecules in the sample. [58]

First, the GST-column was prepared. 5 ml of Glutathione Sepharose 4 Fast Flow was transferred to the column and washed with 15 ml of water and 15 ml of buffer for GST chromatography (Tab. XVI) to wash out the ethanol and equilibrate the column with purification buffer.

Table XVI. Buffer for GST chromatography

Buffer contents	
Tris pH 7.5	20 mmol dm^{-3}
NaCl	500 mol dm^{-3}
EDTA	1 mmol dm^{-3}
DTT	10 mmol dm^{-3}
glycerol	10 %

The slurry was transferred to the glass beaker using a plastic pipette and mixed with the centrifuged sonicate. Together, it was incubated 40 min at 4 °C with constant stirring to adsorb GST-CCNY into the slurry. After incubation, the slurry was transferred back to the column and washed with 300 ml GST buffer to remove all unbound proteins and other molecules.

The presence of C-terminal bound GST was unfavorable in the further usage of the protein. Therefore, in the fusion protein sequence, there was a cleavage site for the PreScission protease between the N-terminal GST and the desired CCNY. When

the protein is removed from the slurry, GST remains bound and cleaved CCNY can be washed from the column. Therefore, the washed slurry with 5 ml GST buffer was transferred to a small beaker. 20 μl of the slurry was taken as a sample before cleavage and PreScission protease (10 U / 1 mg of protein) was added. The mixture was incubated for 2 h at 4 °C with constant stirring to remove the CCNY from the GST tag.

After 2 hours, the 20μl sample after cleavage was taken and the cleavage was verified using SDS PAGE. Into 20μl samples, 5 μl of the sampling buffer (Tab. A.18 on page 89) was added, the samples were heated for 5 min at 95 °C and 20 μl was loaded on the polyacrylamide gel (Tab. A.19 on page 89). SDS PAGE was performed for 1 h at 200 V in 1× SDS buffer (Tab. X on page 41) and the resulting gel was stained with the staining dye (Tab. A.23 on page 90). The slurry was transferred back to the column using a plastic pipette and 10 ml of flow through was collected, mixed, and used for further purification.

The bound GST was eluted from the column using 15 ml elution buffer (Tab. XVII) and the column was regenerated using 4 column volumes (CV) of 70% ethanol, 5 CV 1× PBS pH 7.3, 2 CV 6 mol dm^{-3} guanidine hydrochloride, and 5 CV 1× PBS pH 7.3. The regenerated column was stored in 20% ethanol.

Table XVII. GST elution buffer

Buffer contents	
Tris pH 7.5	20 mmol dm^{-3}
NaCl	500 mol dm^{-3}
EDTA	1 mmol dm^{-3}
DTT	10 mmol dm^{-3}
glycerol	10 %
glutathione	10 mmol dm^{-3}

Size exclusion chromatography

Size exclusion chromatography (method described in Section 2.2.2 on page 43) was performed using a Superdex 75 HiLoad 26/600 column and FPLC at flow rate 2 ml/min. The contents of the purification buffer are in the Tab. XVIII on page 47. Fractions were collected during purification. The presence and purity of the purified CCNY was confirmed by SDS PAGE. Into 20μl samples from each fraction, 5 μl of the sampling buffer (Tab. A.18 on page 89) were added, the samples were heated for 5 min at 95 °C and 20 μl was loaded on the polyacrylamide gel (Tab. A.19 on page 89). SDS PAGE was performed for 1 h at 200 V in 1× SDS buffer (Tab. X on page 41) and the resulting gel was stained with the staining dye (Tab. A.23 on page 90). In the end, fractions containing protein were mixed and concentrated.

Table XVIII. Buffer for size exclusion chromatography

Buffer contents	
Tris-HCl pH 7.5	$50\,\mathrm{mmol\,dm^{-3}}$
NaCl	$150\,\mathrm{mmol\,dm^{-3}}$
EDTA	$1\,\mathrm{mmol\,dm^{-3}}$
DTT	$4\,\mathrm{mmol\,dm^{-3}}$
glycerol	10 %

Then, the absorbance was measured using NanoDrop and the concentration and yield of the protein were determined using Eq. 2.4 on page 43 and Eq. 2.5 on page 44. Protein aliquots were stored at − 80 °C.

2.2.4 Phosphorylation of CCNY

Expression of CCNY in E. coli disables post-translational modifications of the protein, such as phosphorylation. For CCNY to interact with 14-3-3 proteins, phosphorylation of specific serine residues is necessary. For this purpose, protein kinase A was used. The consensus sequence for the phosphorylation of proteins by PKA is B-B-X-Ser/Thr, where B is a basic residue (Arg or Lys) and X is any residue [2].

CCNY construct (1–341 with mutations Y98R, S99A, S324A) has five PKA phosphorylation sites. Two of them, S100 and S326, are mentioned in Shetata et al. [5] as 14-3-3 protein binding sites. In the CCNY sequence, there are also three other natural-occurring PKA sites (S83 is 100% phosphorylated, S25 and S66 are 50% phosphorylated).

Phosphorylation of CCNY was performed in size exclusion buffer (Tab. XVIII) with $75\mathrm{mmol\,dm^{-3}}$ ATP and $20\mathrm{mmol\,dm^{-3}}$ $MgCl_2$ using PKA. PKA was added (280 U PKA for 1 mg of CCNY) and the reaction was performed for 5 h at room temperature and overnight in the refrigerator. The next day, ATP was removed by size exclusion chromatography using a Superdex 75 HiLoad 26/600 column and size exclusion buffer (Tab.XVIII) at flow rate 2 ml/min. Fractions were collected during purification. The presence and purity of the pCCNY was confirmed by SDS PAGE. Into 20μl samples from each fraction, 5 μl of the sampling buffer (Tab. A.18 on page 89) was added, the samples were heated for 5 min at 95 °C and 20 μl was loaded on the polyacrylamide gel (Tab. A.19 on page 89). SDS PAGE was performed for 1 h at 200 V in 1× SDS buffer (Tab. X) and the resulting gel was stained with the staining dye (Tab. A.23 on page 90). In the end, fractions containing protein were mixed, concentrated and the protein aliquots were stored at − 80 °C.

2.2.5 Expression and purification of CDK16

Expression

The human wild type CDK16 (1–496) with C-terminal glutathion S-transferase (GST) fusion tag (sequence in Tab. A.13 on page 87 and Tab. A.14, parameters in the Tab. A.15, both on page 88) was expressed in *E. coli* BL21(DE3)-RIPL cells containing pGEX-6P-1 plasmid. Initially, six starting cultures were prepared by mixing 5 ml of sterile LB medium with ampicillin and chloramphenicol to final concentrations of 100 μg/ml. Ampicillin ensures the growth of only cells with the pGEX-6P-1 plasmid. Chloramphenicol resistance is special for the BL21(DE3)-RIPL cells and ensures the transcription of additional tRNA (argU (AGA, AGG), ileY (AUA), proL (CCC), and leuW (CUA) codons) on two additional plasmids. Cultures were inoculated by *E. coli* cells from the glycerol stock (700 μl of cell suspension, 300 μl of sterile glycerol) and incubated overnight at 37 °C, 180 rpm.

The next day, each starting culture was added to 1 liter of sterile LB medium containing 100 μg/ml of ampicillin and 100 μg/ml of chloramphenicol and grown at 37 °C, 180 rpm. Every hour, the OD_{600} of the suspension was measured using pure LB medium as a blank. When OD_{600} reached 0.8 cm^{-1}, the temperature was lowered to 15 °C to preserve the protein that will be produced. Protein production was induced using 1 ml of 0.5 mol dm^{-3} IPTG and the cultures were incubated at 15 °C, 190 rpm overnight.

Cultures grown were centrifuged 20 minutes in 2.073 g and pellets were resuspended in 180 ml lysis buffer (Tab. XV on page 44). Resuspended cells were frozen at − 80 °C.

Cell lysis

Next day, the cells were thawed and incubated with lysozyme (100 μg/ml) and DNase I (250 μl per 100 ml of lysate) for 40 min at 4 °C. The lysozyme hydrolyzes the cellular walls and helps to release the protein, where DNase degrades the cellular DNA and prevents clogging of the purification column. Then phenylmethylsulfonyl fluoride (PMSF) was added (1 ml PMSF per 100 ml lysate) to inhibit serine proteases that may cause degradation of the expressed protein.

The cells were then sonicated (10 s on, 30 s off, 18 min total) in an ice and water bath and the sonicate was centrifuged at 23.000 g for 45 min. A supernatant with the released recombinant protein was used for further purification.

GST chromatography

For the expression of CDK16 fusion, GST chromatography was used (method description in Section 2.2.3 on page 45). First, the GST-column was prepared. 5 ml of

Glutathione Sepharose 4 Fast Flow was transferred to the column and washed with 15 ml of water and 15 ml of GST buffer (Tab. XVI on page 45) to wash out the ethanol and equilibrate the column with purification buffer.

The slurry was transferred to the glass beaker using a plastic pipette and mixed with the centrifuged sonicate. Together, it was incubated 40 min at 4 °C with constant stirring to adsorb GST-CDK16 into the slurry. After incubation, the slurry was transferred back to the column and washed with 300 ml GST buffer to remove all unbound proteins and other molecules.

The presence of C-terminal bound GST was unfavorable in the further usage of the protein. Therefore, in the sequence of the fusion protein there is a cleavage site for the PreScission protease between the N-terminal GST and the desired CDK16. Cleaving the protein bound to the slurry, GST stays bound and cleaved CDK16 can be washed from the column. Therefore, the washed slurry with 5 ml GST buffer was transferred to a small beaker. 20 μl of the slurry was taken as a sample before cleavage and PreScission protease (10 U / 1 mg of protein) was added. The mixture was incubated for 2 h at 4 °C with constant stirring to remove CDK16 from the GST tag.

After 2 hours, the sample after cleavage was taken and the cleavage was verified using SDS PAGE (the method described in Section 2.2.2 on page 40). The slurry was transferred back to the column using a plastic pipette and 10 ml of flow through was collected, mixed, and used for further purification.

The bound GST was eluted from the column using 15 ml elution buffer (Tab. XVII on page 46) and the column was regenerated using 4 column volumes (CV) of 70% ethanol, 5 CV 1× PBS pH 7.3, 2 CV 6 mol dm^{-3} guanidine hydrochloride and 5 CV 1× PBS pH 7.3. The regenerated column was stored in 20% ethanol.

Size exclusion chromatography

Size exclusion chromatography was performed using the Superdex 200 HiLoad 26/600 column and FPLC. The contents of the purification buffer are in the Tab. XVIII on page 47. Fractions were collected during purification. The presence and purity of the purified CDK16 was confirmed by SDS PAGE. Into 20μl samples from each fraction, 5 μl of the sampling buffer (Tab. A.18 on page 89) was added, the samples were heated for 5 min at 95 °C and 20 μl was loaded on the polyacrylamide gel (Tab. A.19 on page 89). SDS PAGE was performed for 1 h at 200 V in 1× SDS buffer (Tab. X on page 41) and the resulting gel was stained with the staining dye (Tab. A.23). In the end, fractions containing protein were mixed and concentrated. The absorbance was then measured using NanoDrop, and the concentration and yield of the protein were determined using Eq. 2.4 on page 43 and Eq. 2.5 on page 44. The protein aliquots were stored at − 80 °C.

2.2.6 Native electrophoresis of CCNY with 14-3-3 proteins

During SDS PAGE, the proteins are denatured, and potential complexes are disrupted. On the contrary, in the native PAGE, the proteins have their native charge at the pH used and are not denatured prior to loading. In native PAGE, proteins are separated according to their different electrophoretic mobilities and the sieving effects of the gel. [55] Therefore, the formation of protein complexes can be observed using native PAGE.

In native PAGE, the formation of complexes of phosphorylated CCNY and 14-3-3 proteins was observed. Unphosphorylated CCNY with 14-3-3 proteins was taken as a control. At first, the samples for native PAGE (in detail in Tab. XIX) without loading dye were prepared in the test tubes. The samples were left to stay for 1 hour in the refrigerator to establish a balance in complex formation. At the same time, the pre-run of the gels was performed at 200 V using 1× TBE buffer (contents in Tab. XX, pH 8.3, gel contents in Tab. A.24). Then sampling buffer (Tab. A.25 on page 90) was added to all test tubes and the samples were left to stay for 10 min. The samples were then loaded onto the gel and run at 170 V in 1× TBE buffer (Tab. XX, pH 8.3) for 4.5 h in the ice–water bath. The gels were stained using the classic staining procedure (Section 2.2.2 on page 40).

Table XIX. Positioning of the samples on the gel in the native electrophoresis of CCNY with 14-3-3 η and 14-3-3 γ (in μl). *Each column 1–8 responds to one well of the native gel.*

	1	2	3	4	5	6	7	8
14.9 μmol dm^{-3} CCNY	11.6	–	–	–	11.6	11.6	–	–
18.2 μmol dm^{-3} pCCNY	–	11	–	–	–	–	11	11
50 μmol dm^{-3} 14-3-3 η	–	–	4	–	3.4	–	4	–
100 μmol dm^{-3} 14-3-3 η	–	–	–	4	–	3.4	–	4
1× TBE buffer	3.4	4	11	11	–	–	–	–
loading dye	5	5	5	5	5	5	5	5

Table XX. 10× TBE buffer

Buffer contents for 1 liter	
Tris	108 g
H_3BO_3	55 g
0.5mol dm^{-3} EDTA	40 ml

2.2.7 Size exclusion chromatography of the CDK16 complexes

The 150μl samples were prepared as follows:

1. 40μmol dm^{-3} 14-3-3 γ,
2. 20μmol dm^{-3} pCCNY,
3. 20μmol dm^{-3} CDK16,
4. 40μmol dm^{-3} 14-3-3 γ with 20μmol dm^{-3} pCCNY,
5. 40μmol dm^{-3} 14-3-3 γ with 20μmol dm^{-3} pCCNY and 20μmol dm^{-3} CDK16.

The samples were incubated in the refrigerator for 30 min, centrifuged for 5 min at 18.620 g and in each run, 50 μl of the particular sample was loaded to the Superdex 200 Increase 10/300 column. The chromatography was provided at 21 °C in the size exclusion buffer (Tab. XXI) at the flow rate 0.5 ml/min. The 0.25 ml fractions were collected and from the peak fractions, 20μl samples were taken. Into each sample, 5 μl of the sampling buffer (Tab. A.18 on page 89) was added and the samples were heated at 95 °C for 5 min. 20 μl of the samples were loaded to the 12% polyacrylamide gel, the SDS PAGE was performed for 1 h at 200 V in 1× SDS buffer (Tab. X on page 41) and the resulting gel was stained by the staining dye (Tab. A.23 on page 90).

Table XXI. Buffer for size exclusion chromatography

Buffer contents	
Tris pH 7.5	25 mmol dm^{-3}
NaCl	150 mmol dm^{-3}
EDTA	1 mmol dm^{-3}
DTT	2 mmol dm^{-3}
glycerol	10 %

The data from the chromatograms were exported and normalized by subtracting the lowest value of absorbance. As a result, graphs were plotted containing the chromatograms of single proteins and binary and ternary complexes, respectively.

2.2.8 Refinement of the 14-3-3 gamma crystal structure

X-ray crystallography

X-ray crystallography is the widely used tool in structural biology [59] that allows the study of the structure of proteins and protein complexes with atomic resolution.

The physical background of the method is the X-ray diffraction on the atoms of the protein crystals and the interpretation of the measured diffraction patterns. There are two important reasons why structural biologists use X-ray waves and biomolecular crystals. For electromagnetic radiation to diffract on an object, its wavelength must be comparable to the size of the object. In case of biomolecular crystals, we use X-rays of wavelength about 10^{-10} m. Crystals are used as the amplifiers of the intensity of the measured signal (the diffraction measured on a single biomolecule would be too weak). [60, 61] The procedure of the classic crystallographic experiment is as follows:

First, the protein must be produced and purified and high-quality crystals must be created using different crystallographic techniques. First attempts are usually based on a trial-or-error procedure, using a highly pure protein sample with various buffers, salts, precipitants, temperature, and additives. The standard crystallization procedure uses the hanging or sitting drop with protein and precipitant in a closed container with a buffer reservoir with higher salt concentration. The vapor that diffuses from the drop goes to the reservoir, and the concentration of the protein in drop is constantly growing, until crystallization begins. After the crystals are of sufficient quality, the crystals are frozen and used for the diffraction experiment.

Then, a diffraction experiment is conducted and the intensities of the X-ray waves diffracted by the crystal are measured. The X-ray waves are generated by either an X-ray tube or by a synchrotron. During the experiment, the crystal is placed on the goniometer, which allows the crystal to rotate and the complete data set to be collected. The resulting diffraction pattern is further processed to obtain the electron density and a model of the biomolecular structure. [62]

The Bragg's equation

$$2dsin(\theta) = n\lambda \tag{2.6}$$

defines the conditions under the diffracted waves interfere constructively (d is the distance between planes that diffract electromagnetic waves, θ is the diffraction angle and $n\lambda$ is the whole number multiple of the wavelength of the used X-rays). The reflection (and a spot in the diffraction pattern) is only visible for the angles that fulfill Bragg's law. Simultaneously, for the given experimental setup, only the atoms laying on the planes fulfilling Bragg's law are visible. When the distance between the planes is small, the resulting data have a high resolution. The smaller d, the greater is the angle θ, therefore, the spots in the outer part of the diffraction pattern have the highest resolution.

The scattering of the electromagnetic wave on the single atoms is expressed using the atomic scattering factor f:

$$f = 4\pi \int_0^\infty \rho(r) \frac{sin\, kr}{kr} r^2\, dr, \tag{2.7}$$

where $\rho(r)$ is the distribution of the electron density in the atom and $k = \frac{4\pi}{\lambda} sin(\theta)$. When the unit cell contains more atoms j with the scattering factors f_j, the total amplitude of the wave diffracted by the plains hkl is then given by the structure factor F_{hkl}:

$$F_{hkl} = \sum_j f_j e^{2\pi i(hx_j + ky_j + lz_j)}, \tag{2.8}$$

where f_j are the scattering factors of the individual atoms in the elementary cell and the sum is calculated over all atoms of the elementary cell. Millers indexes hkl characterize the planes of the crystal that fulfill the Bragg's law and where the waves interfere constructively. Therefore, this planes are determined as the diffracting planes.

In principle, the structure factors can be calculated from the measured diffraction patterns, because the measured reflection intensity I_{hkl} is equal to $|F_{hkl}|^2$. If all structural factors are known, the distribution of the electron density can be calculated using the equation

$$\rho(r) = \frac{1}{V} \sum_{hkl} F_{hkl} e^{-2\pi i(hx+ky+lz)}, \tag{2.9}$$

where V is the volume of the elementary cell. Actually, in this procedure there is one problematic point that is called the phase problem. F_{hkl} is a complex number $|F_{hkl}|e^{i\alpha}$, where $|F_{hkl}|$ is the amplitude that can be calculated from the experimental data and α is the phase that is not measured. [61] The Eq. 2.9 can therefore be written as

$$\rho(r) = \frac{1}{V} \sum_{hkl} |F_{hkl}| e^{-2\pi i(hx+ky+lz-\alpha)}, \tag{2.10}$$

where α is the phase that is unknown. Without the phase, the distribution of the electron density cannot be calculated. For the solution of the phase problem, more different techniques are used. In the isomorphous replacement, strongly diffracting heavy-atom derivatives of the protein crystals are prepared, and the diffraction data are compared with those of the "normal" crystals. The method of molecular replacement (Section 2.2.8) uses the solved structure of a similar molecule, where anomalous scattering takes advantage of the capacity of the heavy atom to absorb X-rays of the specified wavelength. Using combinations of these methods, the phases of the individual structural factors can be estimated with sufficient accuracy to construct the first electron density map.

The first electron density map is often very noisy but can be improved by different density modification techniques. Then, the protein model can be built and improved by refinement. The quality of the model is checked using the R factor (Section 2.2.8 on page 54) and also visually, using different crystallographic software. At the end, the result of the whole procedure is a protein model in the format of a PDB file

that can be deposited into the protein database or further used for other analyses. [60, 62]

From the whole crystallographic procedure, the final step was performed in this thesis, which is refinement of the build model to be consistent with the measured electron density map as well as the chemical reality of the protein structure.

Molecular replacement

The method of molecular replacement can be used when there is a solved structure of a protein that has a similar structure. When the protein with a solved structure and our protein with an unknown structure has sufficient sequence similarity, the known protein can be used as a phasing model. Simply, the known protein is placed in the unit cell of the new protein, and its known phases are used as the initial phases of the new protein. The phases of the known protein and the amplitudes measured for the new protein are then used for calculation of the first electron density map. [60] For this procedure, many automated softwares can be used, such as MOLREP or Phaser. [63]

Model refinement

When the electron density map is clear enough and the protein model is built, a new structural factor is calculated using Eq. 2.8 on page 53, while treating each atom in the current model as an independent scatterer. The calculated structural factor F_c contains additional information from the model, the properties of the proteins known prior, such as the lengths and angles of the bonds. Combining the measured and calculated structural factors, two electron density maps are calculated that are used for the refinement and building of the protein model:

1. An electron density map calculated using equation

$$\rho(x,y,z) = \frac{1}{V}\sum_{hkl}(|F_o| - |F_c|)e^{-2\pi i(hx+ky+lz-\alpha_{calc})}, \tag{2.11}$$

   where $\rho(x,y,z)$ is an electron density in x,y,z coordinates, V is volume of the elementary cell, $|F_o|$ equals $(I_{hkl})^{1/2}$ where I_{hkl} is the measured intensity from the data set, $|F_c|$ is the structure factor calculated from the model and α_{calc} is the calculated phase. This map is called a $F_o - F_c$ or an electron density-difference map and contains both positive and negative density. Positive density means that the observed intensities (that in F_o) are larger than those of the model (F_cs) and, probably, some atoms of the real protein molecule are absent in the model. The negative density means quite the opposite: the F_cs density is larger than the F_os, and in the model there are some atoms that

are not in the real molecule. This map is very useful for later improvements of the map when the model is quite good but can be very noisy at the beginning of the refinement procedure. That is why the map calculated using Eq. 2.12 is so useful.

2. The electron density map calculated using equation

$$\rho(x,y,z) = \frac{1}{V}\sum_{hkl}(2|F_o| - |F_c|)e^{-2\pi i(hx+ky+lz-\alpha_{calc})} \tag{2.12}$$

is called $2F_o - F_c$ or the "all-features" map. The influence of the model on this map is smaller but still important. Usually, this map is everywhere positive and shows the electron density of the whole molecular surface. Using this map, we can model and fit the molecule to better respond to the measured intensities. [60]

Using automatized refinement software and visualizing the results in a graphical interface, the quality of the electron density map and of the model can be improved in the iterative process called refinement. Nowadays, refinement is mainly an automated process using powerful software packages (e.g. phenix.refine). Choosing different restraints, constraints, and other parameters and a combination of minimizing and simulated annealing, together with manual modeling of problematic parts of the structure (usually first and last residues in the protein chain and less structured loops), makes a final model at the end of the procedure. [64, 65, 60]

After each refinement step, the quality of the model is evaluated by the factor R and the free factor R (R_{free}). Both values are given by the equation

$$R = \frac{\sum_{hkl}||F_o| - |F_c||}{\sum_{hkl}|F_o|}. \tag{2.13}$$

The smaller both are, the better quality of the model. Therefore, the refinement strategy is chosen so that the factor R decreases during the process. The difference between them is in the calculation method. The factor R simply compares the amplitudes of the measured structure factors $|F_o|$ with the amplitudes of the structure factors calculated from the current model $|F_c|$. But the amplitudes used for the evaluation were used for the calculation of the model before. Therefore, in some situations, the R factor can also decrease in the case of overfitting or misfitting the data so that the resulting structure is model biased. In contrast, in the case of R_{free}, a small set of measured amplitudes chosen by random selection is left aside and is not used for refinement. After each refinement step, the difference between the calculated amplitudes and the amplitudes of this evaluation set is compared. Therefore, the evaluation using R_{free} tends to be less model-biased and is more reliable. [60, 66]

Refinement of 14-3-3 gamma

The complex of 14-3-3 γ with 14-3-3 binding site of the CCNY mimicking peptide (sequence `RKRSApSADNL`, where pS is a phosphorylated serine) was crystallized, and the diffraction data was measured and processed by other collaborators (parameters and data are not presented in this thesis). The phase problem was solved using molecular replacement by a previously solved 14-3-3 γ structure (PDB code 2B05), the work was done by the supervisor). The resulting model was refined using the package phenix.refine [67, 68, 65] and Coot software [69] for manual refinement.

The first refinement steps were performed only on the 14-3-3 molecule without peptide. At first, the model was refined using the XYZ refinement strategy in both real and reciprocal space, individual B factors and in some of the cycles was also used simulated annealing (both Cartesian and torsion angles, Fig. 11). In the first attempts, the structure was also controlled and updated manually, especially in poorly structured loops between Thr70–Gly74 and Leu211–Ser215.

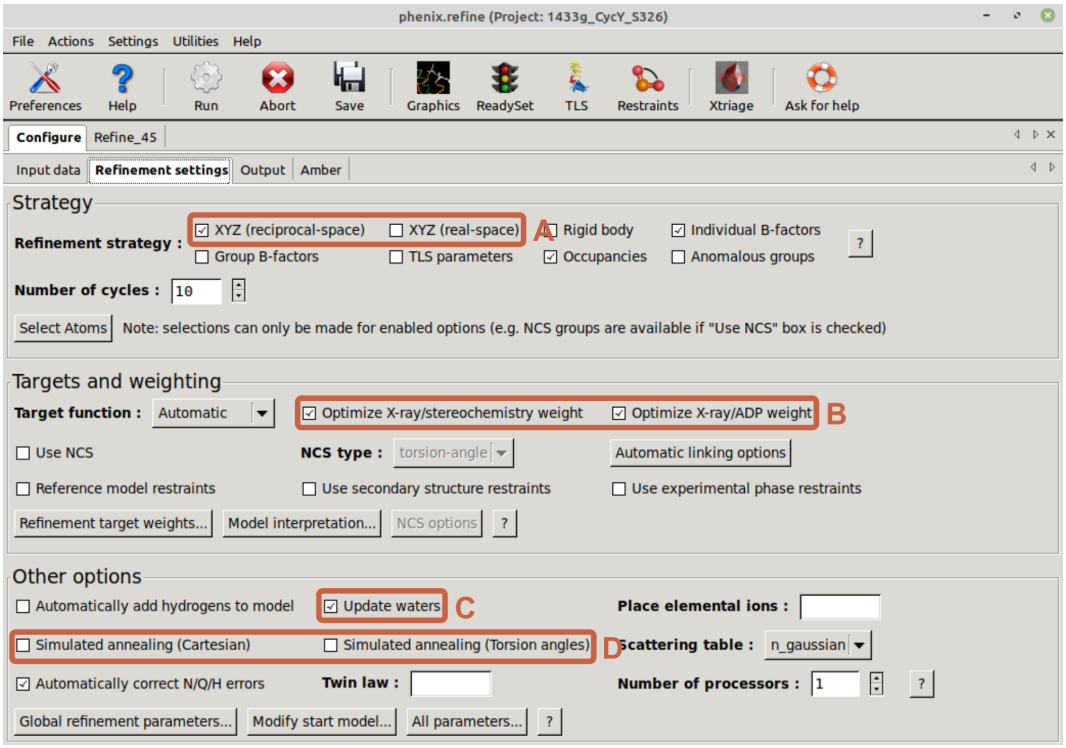

Figure 11. phenix.refine with chosen parameters. ***A.*** *Refinement strategy in XYZ (real and reciprocal space).* ***B.*** *Optimization of X-ray/stereochemistry weights and X-ray/ADP weights.* ***C.*** *Update water molecules.* ***D.*** *Simulated annealing (Cartesian and torsion angles).*

When the quality of the 14-3-3 protein model was sufficient, the peptide was built manually in Coot according to its known sequence. The model with peptide molecules was refined again with similar parameters, and its correspondence to the

measured electron density was checked and optimized manually.

The quality of the model after the next refinement steps was controlled by R_{free} and also using the MolProbity validation tool [68]. The goal was to minimize the number of rotamer and Ramachandran outliers (the conformations of the side chains that did not comply with the values that are known for real proteins) and clashscore (number of atoms that are close enough to be connected by a covalent bond, although there is no bond between them). As a refinement strategy, the XYZ reciprocal space was used. Furthermore, the Optimize X-ray/stereochemistry weights and the Optimize X-ray/ADP weights were on (Fig. 11 on page 56).

At the end of the refinement, the water molecules were added to Coot and the refinement was performed using the update water tool. Redundant waters were removed in Coot, and the final refinement cycle was run.

Chapter 3

Results

3.1 Fluorescence anisotropy

At first, the affinity of all 14-3-3 isoforms for the 14-3-3 binding motifs of CCNY was measured using fluorescence anisotropy. For measurements, three synthetic peptides were used, mimicking two phosphorylated 14-3-3 binding sites (pS100, parameters in the Tab. A.1 and pS360, parameters in the Tab. A.2, both on page 83) and one unphosphorylated 14-3-3 binding site (S100, parameters in Tab. A.3 on page 83). The measurement was performed with two aims: to compare the binding affinities of the individual isoforms to the peptides and also to determine if 14-3-3 isoforms can also bind to unphosphorylated binding sites.

For each isoform and each peptide, a dilution series of 50nmol dm^{-3} peptide and 80 to $1 \cdot 10^{-3}$ μmol dm^{-3} 14-3-3 isoform was measured in triplicates. Results were averaged, plotted, and fitted to a one-site binding model to determine the dissociation constants for the individual combinations of peptides and isoforms (Fig. 12 on page 60).

In Figs. 12 A and B on page 60, the interactions of individual 14-3-3 isoforms with the phosphorylated peptides pS100 and pS360 are visualized, respectively (the dissociation constants are listed in Tab. XXII on page 61). From the data presented, it is visible that the pS100 peptide binds the 14-3-3 γ isoform with the highest affinity (the dissociation constant of the 14-3-3 γ–pS100 peptide complex is 0.199 μmol dm^{-3}) where with the second highest and almost comparable affinity binds the 14-3-3 η isoform (K_D is 0.282 μmol dm^{-3}). The second motif is bound about 20–100× weaker but the isoform preferences are similar: the 14-3-3 η isoform bind with the highest affinity (the dissociation constant of the 14-3-3 η–pS326 peptide complex is 4.7 μmol dm^{-3}) and with the second highest and almost comparable affinity binds the 14-3-3 γ isoform (K_D is 5.9 μmol dm^{-3}). The other isoforms bind to the peptides with significantly lower affinity (for both peptides, the dissociation

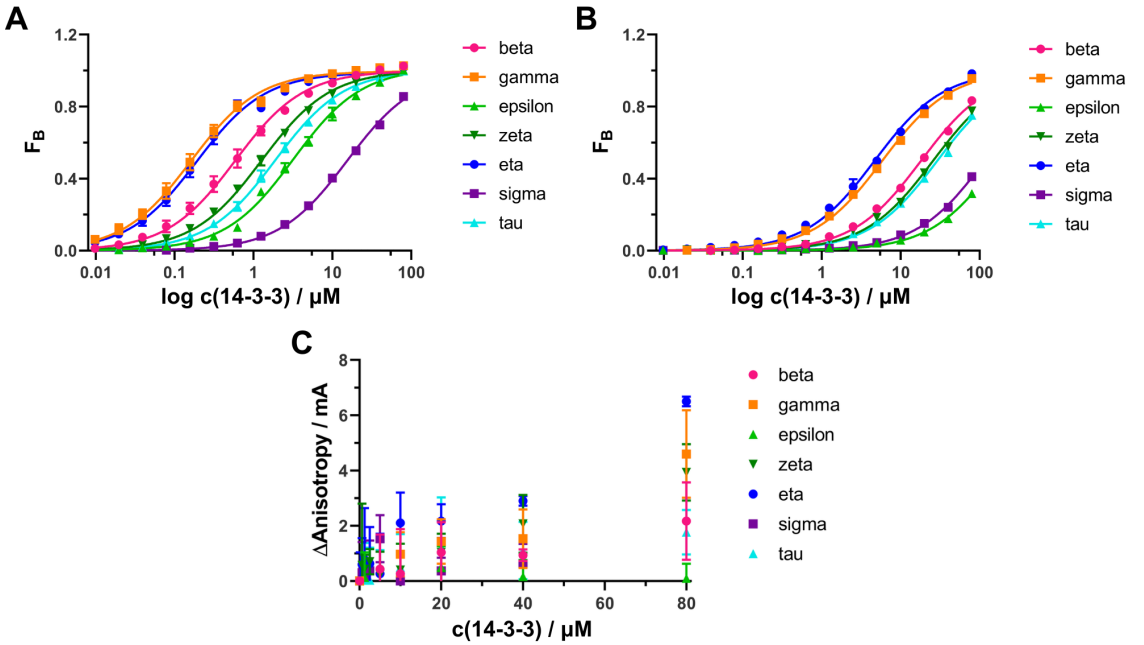

Figure 12. Fluorescence anisotropy of 14-3-3 isoforms with the 14-3-3 binding motifs of CCNY. *The averaged values were fitted to a one-site binding model in the software GraphPad (error bars are not visible if they are smaller than the size of the symbol).* ***A.*** *14-3-3 isoforms with phosphorylated pS100 peptide. F_B is $\Delta A/\Delta A_{max}$. The highest affinity has the γ isoform (in orange, K_D is 0.199 µmol dm^{-3}).* ***B.*** *14-3-3 isoforms with phosphorylated pS326 peptide. F_B is $\Delta A/\Delta A_{max}$. The highest affinity has the η isoform (in blue, K_D is 4.7 µmol dm^{-3}).* ***C.*** *14-3-3 isoforms with unphosphorylated pS100 peptide. The affinities were too low to calculate the ΔA_{max} and K_D values.*

constants of the other 14-3-3–peptide complexes are at least twice higher). Therefore, 14-3-3 η and 14-3-3 γ were chosen as the preferable 14-3-3 protein isoforms for future experiments.

In Fig. 12 C, the interaction of 14-3-3 isoforms with the unphosphorylated S100 peptide is presented. Contrary to phosphorylated peptides, the formation of peptide–14-3-3 protein complexes is not observed and the dissociation constants cannot be determined. This measurement confirmed that unphosphorylated CCNY does not interact with 14-3-3 isoforms.

3.2 Recombinant protein preparation

For the biophysical characterization of the interactions between 14-3-3 η and 14-3-3 γ, CCNY and CDK16, all proteins must have been produced and purified in sufficient amounts and purity for future experiments. This section describes the expression and purification steps for all the desired proteins.

Table XXII. Dissociation constants of the 14-3-3 protein isoforms with CCNY 14-3-3 protein binding sites peptides (in $\mu mol\,dm^{-3}$).

Isoform	K_D
beta	0.59 ± 0.05
gamma	0.199 ± 0.015
epsilon	2.8 ± 0.2
zeta	1.24 ± 0.07
eta	0.282 ± 0.016
sigma	15.4 ± 0.9
tau	1.8 ± 0.1

(a) *14-3-3 isoforms with pS100 peptide.*

Isoform	K_D
beta	18.2 ± 1.4
gamma	5.9 ± 0.3
epsilon	170 ± 40
zeta	26 ± 2
eta	4.7 ± 0.4
sigma	117 ± 17
tau	29 ± 3

(b) *14-3-3 isoforms with pS326 peptide.*

3.2.1 Expression and purification of 14-3-3 eta

14-3-3 η was expressed in *E. coli* cells cultivated in 3 l of LB medium and purified using nickel chelating chromatography, anion exchange chromatography and size exclusion chromatography. LB medium containing ampicillin was inoculated by overnight cultures containing *E. coli* cells and cultivated in a shaker. The expression of 14-3-3 η was induced using IPTG and performed overnight. The recombinant protein was released from the cells by lysozyme and sonication, and the redundant cellular components were removed by centrifugation.

The supernatant was used for the first purification step, the nickel chelating chromatography. The recombinant 14-3-3 η containing Histag was loaded and bound to the nickel chelating column. The unwanted proteins and cellular components were washed with washing buffer. Thereafter, the Histag protein was eluted from the column using a high concentration of imidazole. The purity and amount of the purified protein were confirmed using SDS PAGE (Fig. 13 A on page 62). Fractions containing high amount of 14-3-3 η were mixed and used for the next purification steps. Before that, the concentration of imidazole in the protein sample was lowered by dialysis and the Histag was cleaved using TEV protease. The cleavage was confirmed by comparing a sample before and after cleavage using SDS PAGE (Fig. 13 B on page 62).

The next purification step, anion exchange chromatography, was performed using a Q column to separate the cleaved 14-3-3 η and the TEV protease. Both proteins were eluted by increasing the ionic strength by the gradient of NaCl concentration (Fig. 14 on page 62). The fractions containing 14-3-3 η were collected, mixed and used for the final purification step.

As the last purification step, size exclusion chromatography was performed (Fig. 15 on page 63). The purity and amount of the 14-3-3 η was confirmed using SDS

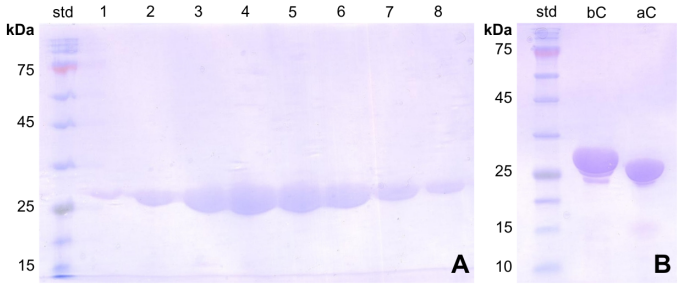

Figure 13. A. The 15% polyacrylamide gel stained by the Coomassie brilliant blue R 250 after the SDS PAGE of the samples from the fractions eluted during the Histag purification of 14-3-3 *η*. *Well marked as std contained 3 µl of the protein standard, wells 1 to 8 contained samples from the collected fractions.* ***B. Comparison of the samples before (bC) and after TEV cleavage (aC) on the SDS PAGE gel.*** *The wells bC and aC contained 3 µl of the protein sample before and after cleavage, the well marked as std contained 3 µl of the protein standard. The 14-3-3 η before cleavage has about 30 kDa, and after cleavage about 28 kDa. On the gel, the higer molecular weight of the uncleaved protein in the bC column compared to lower molecular weight of the cleaved protein in the aC column is visible.*

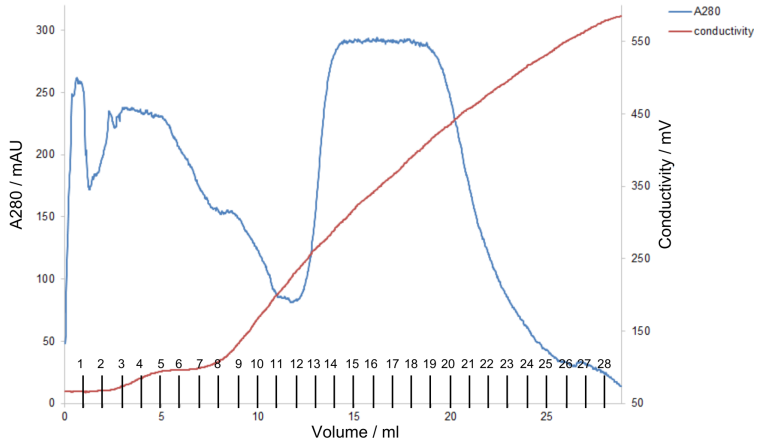

Figure 14. Chromatogram displaying the anion exchange chromatography of 14-3-3 *η*. *On the x-axis is the volume of the mobile phase (in ml) and the collected fractions (in black). On the left y-axis is the absorbance at 280 nm (in mAU, blue), that is proportional to the protein concentration, on the right y-axis is the conductivity (in mV, red), proportional to the increasing concentration of NaCl in the mobile phase. The chromatography was performed using Mono Q column. Fractions containing the 14-3-3 η were mixed and used for the next purification steps.*

PAGE (Fig. 15). The purity of the fractions visible on the SDS PAGE gels is sufficient for biophysical characterization. The fractions containing the 14-3-3 η were mixed and the concentration was measured using NanoDrop. As a result, 47 mg of pure 14-3-3 η was yielded.

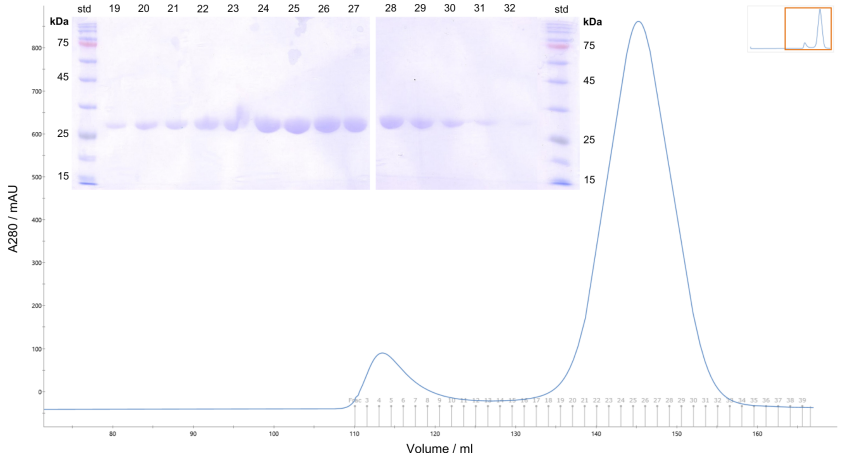

Figure 15. Chromatogram displaying the size exclusion of 14-3-3 η. *The absorbance (that is proportional to the protein concentration, in mAU, displayed in blue) depending on the volume of the mobile phase (in ml). The collected fractions are displayed in gray. For the purification, the Superdex 75 HiLoad 26/600 column was used. The samples of the fractions 19 to 32 were loaded on the 15% polyacrylamide gel and the purity of the protein was confirmed using SDS PAGE. The gel is stained with Coomassie brilliant blue R 250. Well marked as std contained 3 µl of the protein standard. Fractions containing sufficient amount of the pure protein were mixed, concentrated and stored.*

3.2.2 Expression and purification of 14-3-3 gamma

14-3-3 γ was expressed in *E. coli* cells cultivated in 3 l of LB medium and purified using nickel chelating chromatography, anion exchange chromatography and size exclusion chromatography. LB medium containing ampicillin was inoculated by overnight cultures containing *E. coli* cells and cultivated in a shaker. The expression of 14-3-3 γ was induced using IPTG and performed overnight. The recombinant protein was released from the cells using lysozyme and sonication, and the redundant cellular components were removed by centrifugation.

The supernatant was used for the first purification step, the nickel chelating chromatography. The recombinant 14-3-3 γ containing Histag was loaded and bound to the nickel chelating column. The unwanted proteins and cellular components were washed with washing buffer. Thereafter, the Histag protein was eluted from the column using a high concentration of imidazole. The purity and amount of the purified protein were confirmed using SDS PAGE (Fig. 16 A on page 64). Fractions

containing high amounts of 14-3-3 γ were mixed and used for the next purification steps. Before that, the concentration of imidazole in the protein sample was lowered by dialysis and the Histag was cleaved using TEV protease. The cleavage was confirmed by comparing a sample before and after cleavage using SDS PAGE (Fig. 16 B).

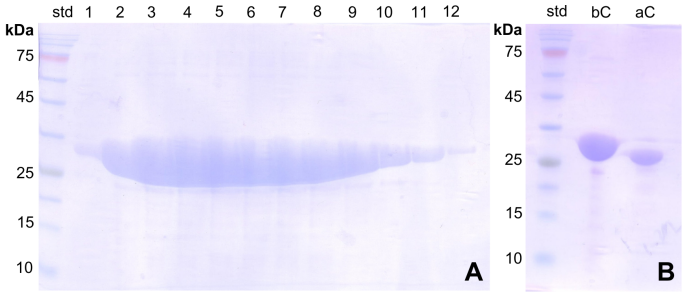

Figure 16. A. The 15% polyacrylamide gel stained by Coomassie Brilliant Blue R 250 after SDS PAGE of the samples from the fractions eluted during Histag purification of 14-3-3 γ. *Well marked as std contained 3 μl of the protein standard, wells 1 to 8 contained samples of the collected fractions.* ***B. Comparison of samples before (bC) and after TEV cleavage (aC) on 15% polyacrylamide gel stained with Coomassie brilliant blue R 250.*** *The wells bC and aC contained 3 μl of the protein sample before and after cleavage. The well marked as std contained 3 μl of the protein standard. The 14-3-3 γ before cleavage has approximately 30 kDa, and after cleavage approximately 28 kDa. On the gel, the higher molecular weight of the uncleaved protein in the bC column is visible compared to the lower molecular weight of the cleaved protein in the aC column*

The next purification step, anion exchange chromatography, was performed using a Q column to separate the cleaved 14-3-3 γ and the TEV protease. Both proteins were eluted by increasing the ionic strength by the gradient of NaCl concentration (Fig. 17 on page 65). The fractions containing 14-3-3 γ were collected, mixed and used for the final purification step.

As the last purification step, size exclusion chromatography was performed (Fig. 18 on page 65). The purity and amount of the 14-3-3 γ was confirmed using SDS PAGE (Fig. 18 on page 65). The purity of the fractions visible on the SDS PAGE gels is sufficient for biophysical characterization. The fractions containing a higher amount of 14-3-3 γ were mixed and the concentration was measured using NanoDrop. As a result, 60 mg of pure 14-3-3 γ was yielded.

3.2.3 Expression and purification of CCNY

The fusion recombinant GST-CCNY was expressed in *E. coli* cells and purified using GST chromatography and size exclusion chromatography. 6 l LB media containing

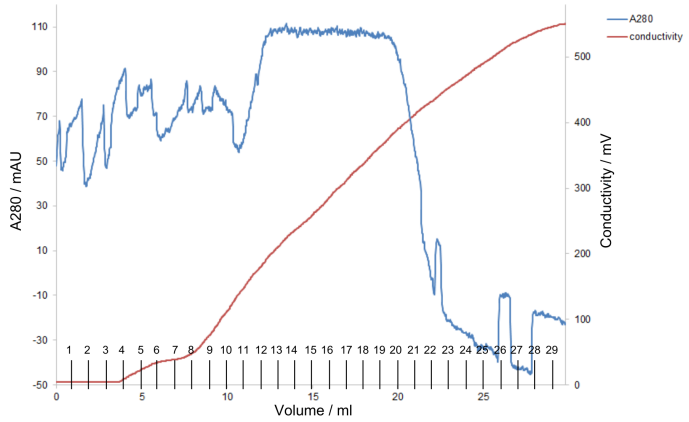

Figure 17. Chromatogram displaying the anion exchange chromatography of 14-3-3 γ. *On the x-axis are the volume of the mobile phase (in ml) and the fractions collected (in black). On the left y-axis is the absorbance at 280 nm (in mAU, blue), which is proportional to the protein concentration, on the right y-axis is the conductivity (in mV, red), proportional to the increasing concentration of NaCl in the mobile phase. Chromatography was performed using the Mono Q column. Fractions containing the 14-3-3 γ were mixed and used for the next purification steps.*

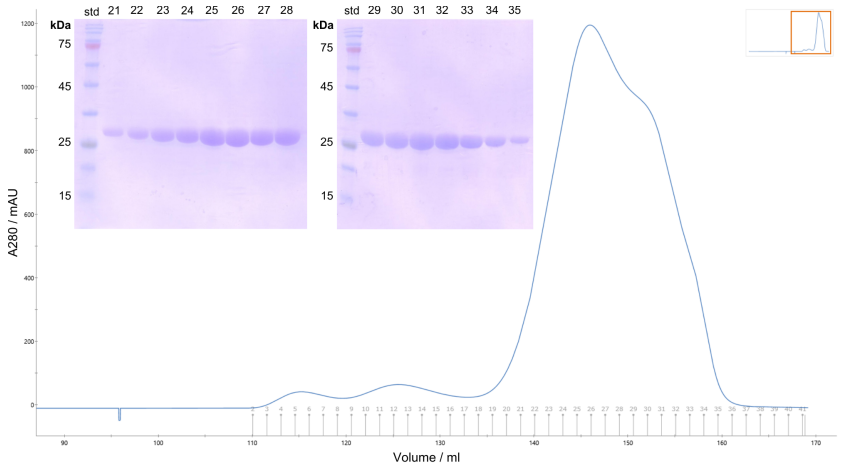

Figure 18. Chromatogram displaying the size exclusion of 14-3-3 γ. *The absorbance (that is proportional to the protein concentration, in mAU, displayed in blue) depends on the volume of the mobile phase (in ml). The fractions collected are shown in gray. For purification, the Superdex 75 HiLoad 26/600 column was used. Samples of fractions 19 to 32 were loaded onto 15% polyacrylamide gel and protein purity was confirmed using SDS PAGE. Well marked as std contained 3 μl of the protein standard. The resulting gel was stained with the Coomassie brilliant blue R 250. Fractions containing a sufficient amount of pure protein were mixed, concentrated, and stored.*

ampicillin and chloramphenicol were inoculated by overnight cultures, cultivated on the shaker, and the expression of CCNY was induced by IPTG addition. The grown cellular cultures were centrifuged, resuspended, and the expressed protein was released by lysozyme and sonication. The redundant cellular components were removed by centrifugation, and the supernatant was used for GST purification.

The GST-CCNY-containing supernatant was mixed and incubated with glutathione sepharose, to bind to the immoilized glutathione. The mixture was then transferred to the column and washed with the purification buffer to remove unbound proteins. For the removal of the GST anchor and release of the CCNY from the glutathione sepharose, the sepharose with bound protein was transferred to a beaker and cleaved by the PreScission protease. Subsequently, glutathione sepharose was transferred back to the purification column and the eluent was collected. The cleavage was confirmed by comparing the sample before and after cleavage using SDS PAGE (Fig. 19).

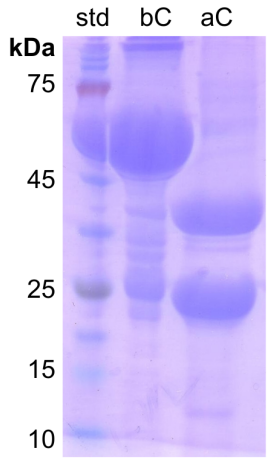

Figure 19. The 15% polyacrylamide gel stained by the Coomassie brilliant blue R 250 after the SDS PAGE of the CCNY sample before (bC) and after TEV cleavage (aC). *Well marked as std contained 3 µl of the protein standard. In the bC column, a huge band of GST-CCNY is visible between 70 and 50 kDa (the molecular weight is about 66 kDa). In the aC column, two bands at approximately 40 kDa nad 26 kDa are visible, where the 40kDa is the cleaved CCNY and 26kDa is the GST.*

The protein eluted from the GST column was used for the final purification step, exclusion chromatography (Fig. 20 on page 67). For protein injection, a 5ml injection loop was used. Due to the problems with aggregation during the concentration of CCNY, the 10ml CCNY sample was purified in two consecutive runs. Subsequently, the amount and purity of the protein in the collected fractions was confirmed using SDS PAGE (Fig. 20 on page 67). The purity of the fractions visible on the SDS PAGE gels was sufficient for further experiments. Fractions containing a higher

amount of CCNY were mixed and concentrated, and the concentration of the final sample was measured. The yield was determined to be 5.4 mg of pure CCNY.

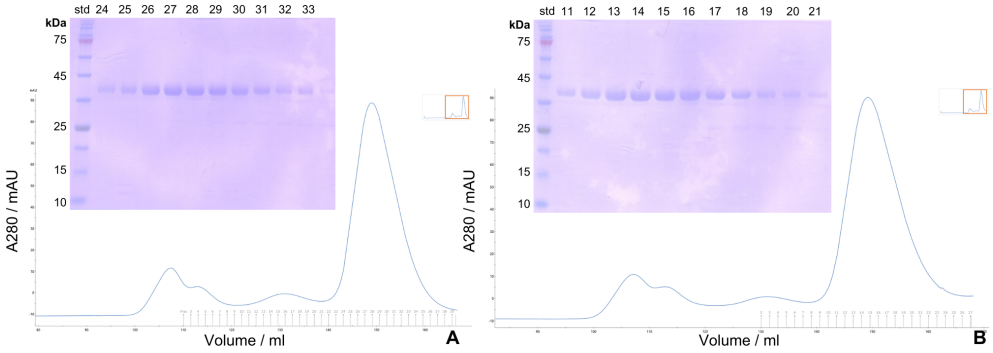

Figure 20. The first (A) and second (B) run of the size exclusion chromatography of CCNY. *In each run, 5 ml of the mixed protein sample containing CCNY was purified. In the both chromatograms, in blue is displayed the absorbance (that is proportional to the protein concentration, in mAU) depending on the volume of the mobile phase (in ml). The collected fractions are in gray. For the purification, the Superdex 75 HiLoad 26/600 column was used. The samples of the fractions 24 to 33 from the first and 11 to 21 from the second run were loaded on the 15% polyacrylamide gel and the purity of the protein was confirmed using SDS PAGE. The resulting gel was stained by the Coomassie brilliant blue R 250. Fractions containing sufficient amount of the pure protein were mixed, concentrated and stored.*

3.2.4 Phosphorylation of CCNY

For CCNY to bind 14-3-3 proteins, the 14-3-3 binding sites must have been phosphorylated. Therefore, half of the produced CCNY was phosphorylated by PKA. The phosphorylation of the CCNY was performed in the size exclusion buffer from the last purification step with added ATP and magnesium chloride, which are necessary for the kinase reaction. After adding PKA, the reaction mixture was incubated for 5 hours at room temperature and then in the refrigerator overnight. The next day, size exclusion chromatography was performed to remove unconsumed ATP (Fig. 21 on page 68). The collected fractions 10 to 20 were mixed, concentrated, and stored for further use.

3.2.5 Expression and purification of CDK16

The recombinant CDK16–GST was expressed in *E. coli* cells and purified in the same way as CCNY by GST chromatography and size exclusion chromatography. 6 l LB media with ampicilling and chloramphenicol were inoculated by the overnight *E. coli* cultures and cells were cultivated on a shaker. The expression of CDK16 was induced by IPTG and the cultures were incubated in the shaker overnight. The

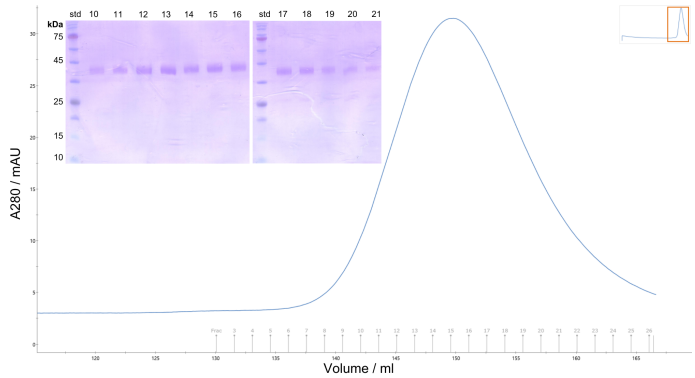

Figure 21. The chromatogram of the size exclusion of phosphorylated CCNY. *Absorbance (proportional to the protein concentration, in mAU, displayed in blue) depends on the volume of the mobile phase (in ml). Collected fractions are displayed in grey. For the purification, the Superdex 75 HiLoad 26/600 column was used. The samples of the fractions 10 to 21 were loaded on the 15% polyacrylamide gel and the purity of the protein was confirmed using SDS PAGE. The resulting gel was stained by the Coomassie brilliant blue R 250. Fractions containing sufficient amount of the pure protein were mixed, concentrated and stored.*

next day, the recombinant protein was released from the cells using lysozyme and sonication and the redundant cellular components were separated from the dissolved proteins by centrifugation. The supernatant containing GST-CDK16 was used for purification.

GST-CDK16 was bound to glutathion sepharose by co-incubation. The mixture was transferred to the column, and the unbound proteins were washed by purification buffer. CDK16 was cleaved from GST by incubation with the PreScission protease in a beaker. After the mixture was transferred back to the column, the cleaved CDK16 was eluted and collected. The cleavage was confirmed by SDS PAGE (Fig. 22 on page 69) of the sample taken before and after cleavage.

The protein sample was further purified using size exclusion chromatography. The resulting fractions were checked by SDS PAGE (Fig. 22 on page 69) and the fractions containing the highest amount of protein were mixed and concentrated. The concentration was measured and the final yield was determined to be 5.3 mg pure CDK16.

3.3 Native electrophoresis

After the expression and purification of all proteins, the interactions between 14-3-3 protein (η and γ isoforms) and CCNY were analyzed. To decide whether 14-3-3 proteins bind to unphosphorylated (CCNY) or phosphorylated CNNY (pCCNY), both or any of them, native electrophoresis of potential (p)CCNY–14-3-3 protein com-

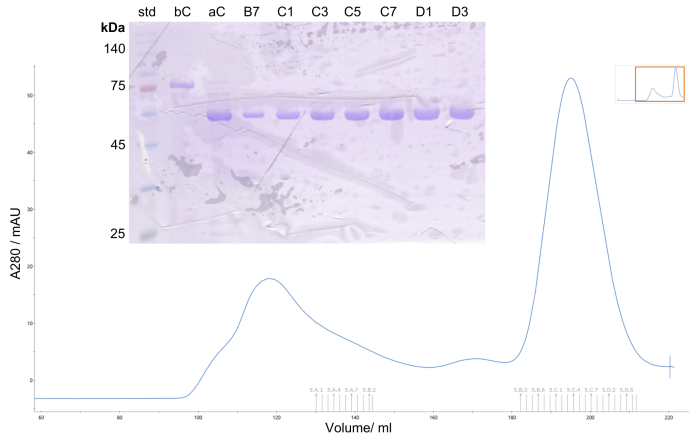

Figure 22. Chromatogram of the CDK16 size exclusion. *Absorbance (proportional to the protein concentration, in mAU, displayed in blue) depends on the volume of the mobile phase (in ml). Collected fractions are displayed in grey. For the purification, the Superdex 200 HiLoad 26/600 column was used. The samples of the chosen fractions between B7 and D3 (all from the right large peak) were loaded on the 12% polyacrylamide gel and the purity of the protein was confirmed using SDS PAGE. The resulting gel was stained by the Coomassie brilliant blue R 250. Fractions containing sufficient amount of the pure protein were mixed, concentrated and stored. Wells marked as bC and aC contain CDK16 samples before and after cleavage. The spot on the gel moved from around 80 kDa before cleavage to around 56 kDa after cleavage.*

plexes was performed. For analysis, both the pCCNY–14-3-3 protein and CCNY–14-3-3 protein samples were used. 14-3-3 proteins dimerize and usually bind in a 1 : 2 ratio (any protein : 14-3-3 proteins), but the interaction between (p)CCNY and the 14-3-3 proteins has been poorly characterized so far. Therefore, the (p)CCNY : 14-3-3 protein molar ratio used for the analysis was both 1 : 1 and 1 : 2. As control samples, individual proteins (CCNY, pCCNY, 1× 14-3-3 and 2× 14-3-3) in the same molar concentrations as in the mixtures. The whole experiment was performed twice, once with the 14-3-3 η and once with 14-3-3 γ isoform.

All samples for the native PAGE were prepared in the test tubes. At first, the samples were incubated for one hour in the refrigerator, so balance in complex formation was achieved. At the same time, the ammonium and persulfate ions unconsumed by the polymerization were washed out by the prerun of the gel. After the incubation of the proteins or protein mixtures, the sampling buffer was added to the test tubes and the samples were incubated for 10 min. The prepared samples were loaded onto the gel and the electrophoresis was performed. Then, the gel was stained using the classic staining procedure and the resulting patterns were analyzed (Fig. 23 on page 70 where A. is (p)CCNY with 14-3-3 η and B. is (p)CCNY with 14-3-3 γ).

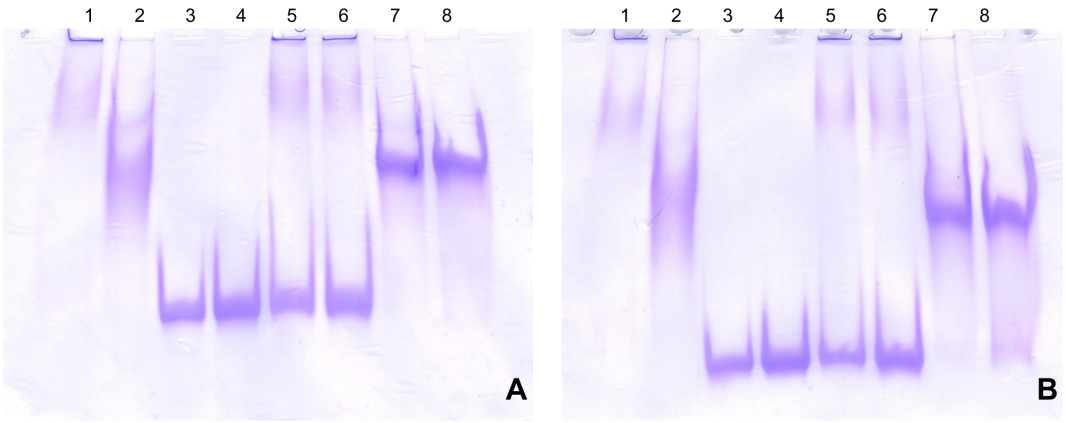

Figure 23. The 12% polyacrylamide gel stained by Coomassie brilliant blue R 250 after the native electrophoresis of the complexes of (p)CCNY with A. 14-3-3 η and B. 14-3-3 γ isoform. *1. Unphosphorylated CCNY. 2. Phosphorylated CCNY (pCCNY). 3. 1× 14-3-3 isoform. 4. 2× 14-3-3 isoform. 5. CCNY with 1× 14-3-3 isoform. 6. CCNY with 2× 14-3-3 isoform. 7. pCCNY with 1× 14-3-3 isoform. 8. pCCNY with 2× 14-3-3 isoform. In the first four columns, the bands of the individual proteins can be recognized. Mostly neutral CCNY moves slowly and stays in the first quarter of the gel. pCCNY is more negative, moves faster, and is visible in the second quarter. Acidic 14-3-3 proteins move rapidly and can be recognized in the third quarter. In the columns with unphosphorylated CCNY with 14-3-3 protein, bands for both individual proteins are visible without further additional band. It confirms that unphosphorylated CCNY does not interact either with 14-3-3 η or with 14-3-3 γ. On the contrary, in the columns containing pCCNY with the 14-3-3 protein, there are no individual bands and there is a new band that does not belong to any of the individual proteins. This confirms the presence of stable pCCNY–14-3-3 η and pCCNY–14-3-3 γ complexes, respectively.*

In the first four columns of both native gels, the bands of the individual proteins can be recognized. Unphosphorylated CCNY, with pI around 7, is at pH 8.3 almost neutral and moves in the gel very slowly. Its band is visible in the first quarter of the gel. pCCNY is five times phosphorylated and each phosphate group carries three negative charges. Therefore, pCCNY is significantly more negatively charged and moves faster. Its band is significantly moved forward, compared to CCNY. 14-3-3 proteins, on the other hand, are acidic with pI around 5. Under experimental conditions, they are strongly negatively charged. Therefore, they move quickly in the gel and their band can be clearly recognized in the third quarter of the gel.

In the next four columns of the gels, the 1 : 1 and 1 : 2 complexes of (p)CCNY with 14-3-3 η and (p)CCNY with 14-3-3 γ are visible. In the first two columns, containing 1 : 1 and 1 : 2 CCNY–14-3-3 protein mixtures, bands are present for the CCNY and 14-3-3 proteins. Also, there are no new bands on both columns. In contrast, in the second two columns, containing 1 : 1 and 1 : 2 pCCNY–14-3-3 protein mixtures, the bands for individual pCCNY and 14-3-3 proteins are not visible. In addition, a new band is visible in the second quarter of the gel, which does not belong to any of the individual proteins. Therefore, it can be assumed that both 14-3-3 η and 14-3-3 γ does not interact with unphosphorylated CCNY in a 1 : 1 or 1 : 2 ratio. On the contrary, both 14-3-3 η and 14-3-3 γ obviously interact with phosphorylated CCNY and both isoforms form with pCCNY a stable binary complex that is clearly recognizable on the native gels.

3.4 Size exclusion chromatography of the CDK16 complexes

The interaction of CDK16, phosphorylated CCNY and 14-3-3 γ was studied using size exclusion chromatography of individual proteins and two different complexes. To confirm the interaction between pCCNY with 14-3-3 γ under the experimental conditions, the binary pCCNY–14-3-3 γ complex was first studied. Then, the whole ternary CDK16–pCCNY–14-3-3 γ complex was characterized.

As a first step, the samples for the size exclusion chromatography were prepared. To obtain comparable results among the individual samples, all samples were prepared with the same volume and concenration of the individual proteins. All samples were incubated at least 30 min in the refrigerator to establish equilibrium in the formation of the complex. The samples were then centrifuged to remove protein aggregates, and size exclusion chromatography of all samples was performed. After chromatography of each sample, samples from fractions of the chromatogram peak were taken. The identity of the proteins of the peak was confirmed using SDS PAGE.

The results are depicted in Fig. 24 on page 72 and Fig. 25 on page 73. To obtain

a comparable result, the values of A_{280} of each chromatogram were normalized by subtracting the lowest value of A_{280}.

In Fig. 24, chromatograms from the size exclusion of 14-3-3 γ, pCCNY and the pCCNY–14-3-3 γ binary complex are displayed. pCCNY, with a size of about 40 kDa, is the smallest protein and elutes at 15.5 ml of the mobile phase. 14-3-3 γ, forming a homodimer of about 57 kDa, elutes at 15 ml of the mobile phase. On the chromatogram from the size exclusion of the pCCNY–14-3-3 γ complex, a single peak indicates that the proteins constitute a 2 : 1 binary complex. The absence of peaks at 15 and 15.5 ml confirms that no unbound proteins are present in the pCCNY–14-3-3 γ sample. The pCCNY–14-3-3 γ complex (approximately 97 kDa) elutes approximately at 14 ml. The SDS PAGE (Fig. 24) from the peak of the complex confirms that in the both 14-3-3 γ and pCCNY are present.

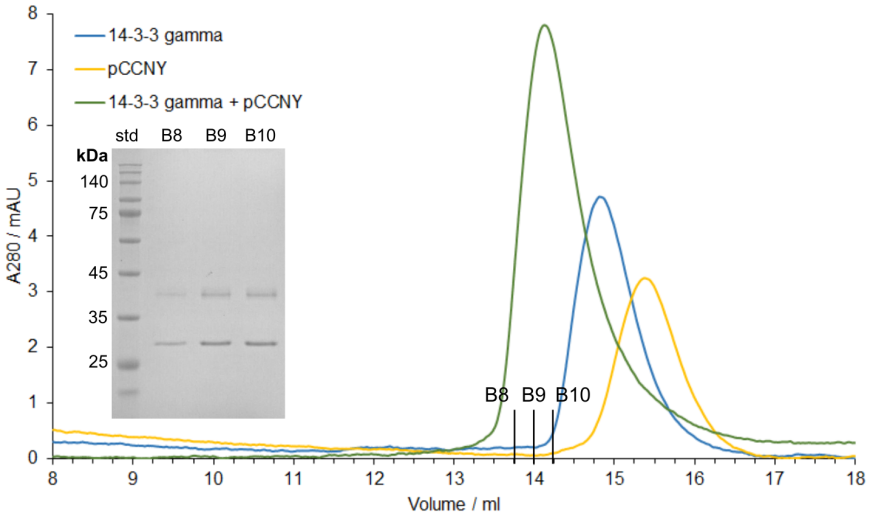

Figure 24. Chromatograms of the size exclusion of 14-3-3 γ (blue), pCCNY (yellow) and its binary complex (green) using the Superdex 200 Increase 10/300 column, and the 12% polyacrylamide gel after SDS PAGE of the samples from the chromatogram peak. *Absorbance (proportional to the protein concentration, in mAU) depends on the volume of the mobile phase (in ml). The fractions collected from the peak are displayed in black. From the green curve, it is visible that the 14-3-3 γ and pCCNY constitute a binary complex of 2 : 1 under experimental conditions, creating a single peak in the chromatogram. In the chromatogram of the 14-3-3 γ–pCCNY complex, no peaks for the individual proteins are visible. On the SDS PAGE gel, the well marked as std contained 3 μl of the protein standard and the other wells contained samples of fractions of the peak of the 14-3-3 γ–pCCNY complex chromatography. In all fractions, both 14-3-3 γ and pCCNY bands are visible, confirming the presence of both proteins in the binary complex.*

In Fig. 25 on page 73, chromatograms are displayed from the size exclusion of 14-3-3 γ, pCCNY, CDK16 and the CDK16–pCCNY–14-3-3 γ teranary complex are

displayed. The smallest pCCNY elutes at about 15.5 ml of the mobile phase, 14-3-3 γ dimer elutes at 15 ml, CDK16 (with the size of 56 kDa) elutes at 14.5 ml. The large peak at 13.5 ml in the chromatogram of the CDK16–pCCNY–14-3-3 γ sample confirms the presence of the 1 : 1 : 2 ternary complex (of a size of 150 kDa). Except for the large peak of the ternary complex, a small peak at 14.5 ml indicates the presence of unbound CDK16 in the sample. The SDS PAGE (Fig. 25) from the peak of the complex confirms that all 14-3-3 γ, pCCNY and CDK16 are present in the complex.

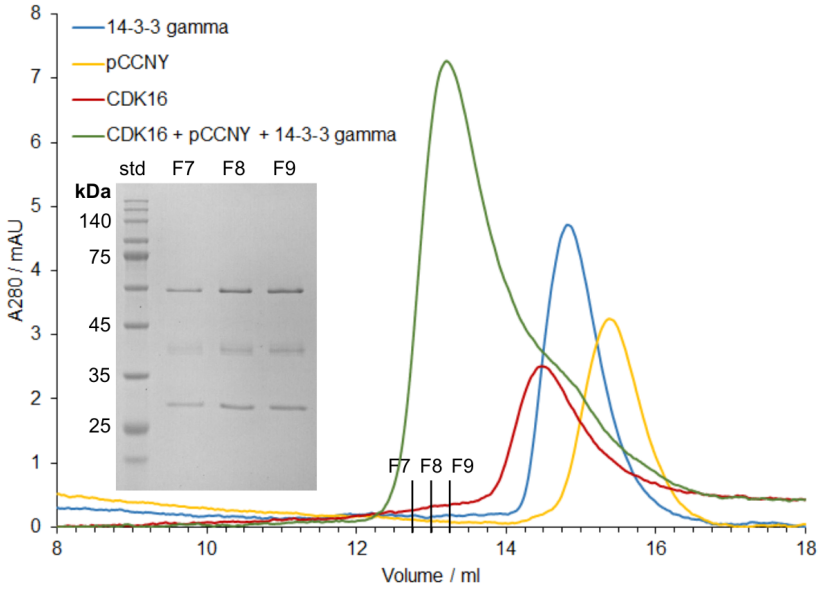

Figure 25. Chromatograms of the size exclusion of 14-3-3 γ (blue), pCCNY (yellow), CDK16 (red) and its ternary complex (green) using the Superdex 200 Increase 10/300 column, and the 12% polyacrylamide gel after SDS PAGE of the samples from the chromatogram peak. *Absorbance (proportional to the protein concentration, in mAU) depends on the volume of the mobile phase (in ml). The fractions collected from the peak are displayed in black. From the green curve, it is visible that the 14-3-3 γ, pCCNY and CDK16 constitute a ternary complex of 2 : 1 : 1 under the experimental conditions, creating a single peak in the chromatogram. In the chromatogram of the 14-3-3 γ–pCCNY–CDK16 complex, no peaks for the individual proteins are visible. On the SDS PAGE gel, the well marked as std contained 3 μl of the protein standard and the other wells contained samples of fractions of the peak of the 14-3-3 γ–pCCNY–CDK16 complex chromatography. In all fractions, all three 14-3-3 γ, pCCNY and CDK16 bands are visible, confirming the presence of all three proteins in the ternary complex.*

3.5 Refinement of the 14-3-3 crystal structure

The 14-3-3 γ in complex with the pS326 14-3-3 binding motif of CCNY was crystallized, the diffraction data were measured and the phase problem was solved by molec-

ular replacement by the collaborators. The structure was refined using phenix.refine software. For all 14-3-3 γ molecules, there was an electron density for the peptide in the binding groove. Therefore, the peptide was built manually and the structure was refined until it reached the parameters in the Tab. XXIII.

Table XXIII. Data collection and refinement statistics. *Statistics for the highest-resolution shell are shown in parentheses.*

Complex 14-3-3 γ with pCCNY pS326 peptide	
Wavelength (Å)	1.54184
Resolution range	25.72–2.201 (2.279–2.201)
Space group	R 3:H
Unit cell	205.743 205.743 74.3405 90 90 120
Total reflections	130637
Unique reflections	58297 (5836)
Multiplicity	2.2
Completeness (%)	97.9 (97.8)
Mean I/sigma(I)	14.52 (1.72)
Wilson B-factor	26.54
R_{meas} (%)	7.3 (41.1)
Reflections used in refinement	58244 (5778)
Reflections used for R-free	2912 (269)
R_{work}	0.2190 (0.2962)
R_{free}	0.2565 (0.3250)
Number of non-hydrogen atoms	8443
Number of macromolecules atoms	7721
Number of ligands atoms	0
Number of solvent atoms	722
Protein residues	967
RMS(bonds)	0.001
RMS(angles)	0.32
Ramachandran favored (%)	99.79
Ramachandran allowed (%)	0.21
Ramachandran outliers (%)	0.00
Rotamer outliers (%)	0.49
Clashscore	1.84
Average B-factor	33.04
B-factor macromolecules	32.79
B-factor solvent	35.70

The structure of 14-3-3 γ with the synthetic pS326 peptide was solved with resolution 2.201 Å (Fig. 26 on page 75) and the resulting R_{free} was 0.257 and 0.325, respectively. Crystals belonged to the space group R 3:H, with four phosphopeptide–

14-3-3 γ complexes in the asymmetric unit. In the solved structure, 99.79 % of the residues are in the Ramachandran-favored conformation, 0.21 % are in the Ramachandran allowed (there are no Ramachandran outliers in the structure). There are 0.49 % of the rotamer outliers and the clashscore is 1.84. In two complexes, two 14-3-3 γ residues were excluded from the model (Val1 and Ala72 in chain A, Val1 and Gly74 in chain B, respectively). In three complexes, the entire phosphopeptide backbone (10 amino acids) could be built to the electron density map, where R321 of the chain F was excluded from the model. In each phosphopeptide, one or two side chains were not built, usually for the first or the last residue.

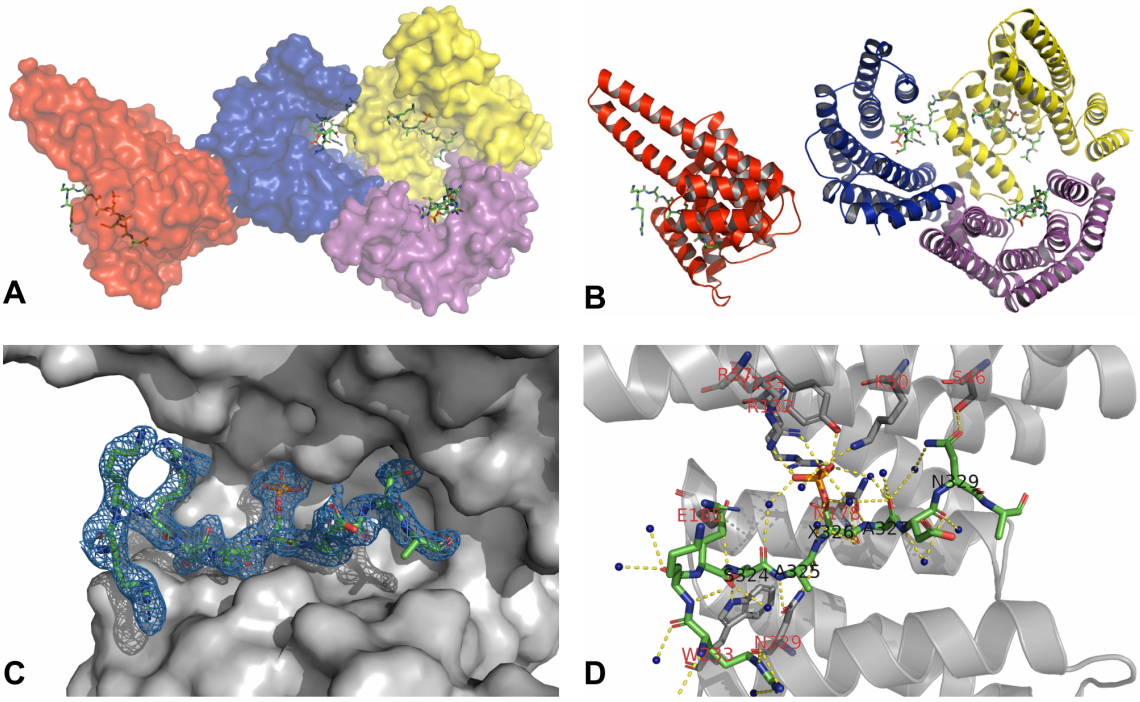

Figure 26. Crystal structure of the 14-3-3-binding motif `RKRSApSADNL` ***of CCNY bound to 14-3-3*** γ***.*** *Surface (**A.**) and cartoon (**B.**) representation of the assymetric unit containing four 14-3-3 γ monomers. The pS326 peptide is shown as green sticks in the binding groove of the each monomer. **C.** pS326 peptide molecule (green) with the $2F_o - F_c$ the electron density map contoured at $\sigma = 1$ (blue). **D.** Polar contacts (yellow dashed lines) between pS326 peptide (green, black labels), 14-3-3 γ (gray, red labels) and water molecules (blue spheres).*

One peptide molecule is bound in each binding groove of all 14-3-3 protomers (Fig. 26 A, B). In Fig. 26 C, the peptide structure is displayed in the 14-3-3 protein binding groove with the electron density map. The polar contacts are depicted in Fig. 26 D. The phosphate group of the pS326 residue forms polar contacts with the side chains of the residues Lys50, Arg57, Arg132, and Tyr133. There are also additional polar contacts between Ser324 of the peptide and Glu185 and Thr233 of the protein, Ala325 of the peptide and Asn229 of the protein, Ala327 of the peptide

and Asn178 of the protein, and Asn329 and Ser46 of the peptide.

Chapter 4

Discussion

CDK16 is a cell-cycle-connected cyclin-dependent kinase [4] that is present exclusively in postmitotic animal cells. CDK16 functions primarily in neurite outgrowth processes, regulation of axonal transport, is essential for spermatozoa development, and plays a role in the progression of X-linked intellectual disability. CDK16, similar to the other CDKs, is activated by its binding partner, CCNY. [18, 5] Although the exact function of CCNY is still unknown, its expression is essential for the development of many organisms. [30]. In addition, it plays a role in the development and progression of different types of cancers. Therefore, CDK16 and CCNY could be potential new therapeutic targets. [31]

Structurally, both CDK16 and CCNY are nontypical among similar proteins. CDK16, except the highly conserved kinase domain, contains N- and C-terminal extensions that play a role in the interaction between CDK16 and CCNY. Moreover, it has a Cys substitution for Ser in the C-helix that plays a major role in the cyclin binding. [4] CCNY contains only one cyclin box fold instead of two, which are present in the typical cyclin structure. In addition, CCNY contains long extension domains at both the N- and C-termini. [6]

The interaction of CDK16 with CCNY requires CCNY to be phosphorylated and bound to 14-3-3 proteins. [5] The 14-3-3 proteins that are studied in our laboratory are dimeric acidic proteins that interact with a large number of other proteins. Seven different isoforms of 14-3-3 proteins are found in human cells, which tend to both homo- and heterodimerization. 14-3-3 proteins play important roles in regulation of many important cellular processes, such as the cell cycle, apoptosis, and autophagy. They enable conformational changes of the proteins and mediate protein-protein interactions. In order to interact with 14-3-3 proteins, their binding partnes have to be phosphorylated. [44, 36] For CCNY to interact with 14-3-3 proteins, phosphorylation of 14-3-3 binding sites S100 and S326 is necessary. [5]

Recent publications indicate that CDK16 is activated by a novel mechanism containing the formation of the CDK16–pCCNY–14-3-3 protein complex. [5] However,

the molecular mechanism of CDK16 activation by the pCCNY and 14-3-3 proteins is not known. The first step for biophysical and structural studies of these interactions is to prepare the relevant proteins and verify their interactions in vitro.

The first step of this thesis was to compare the binding affinities of all human 14-3-3 isoforms for the phosphorylated 14-3-3 binding motifs of human CCNY using fluorescence anisotropy measurements. According to the data presented in Figs. 12 A. and B. on page 60 and in Tab. XXII on page 61, peptide pS100 binds to all 14-3-3 isoforms in the low micromolar range, with the lowest K_D values for the 14-3-3 γ and 14-3-3 η isoforms ($0.199\,\mu\mathrm{mol\,dm^{-3}}$ and $0.282\,\mu\mathrm{mol\,dm^{-3}}$, respectively). The pS326 peptide binds about 20–100× weaker, with the lowest K_D values for the 14-3-3 η and 14-3-3 γ isoforms ($4.7\,\mu\mathrm{mol\,dm^{-3}}$ and $5.9\,\mu\mathrm{mol\,dm^{-3}}$, respectively).

The measured values are in agreement with previous studies of 14-3-3 binding affinities to other peptides that are in similar ranges. In the study by Obsilova et al. [70], the K_D values for the complex of pRaf-259 peptide with 14-3-3 ζ were in the 100nm range, where the K_D values for the Nedd4-2–14-3-3 isoform complexes in the study by Pohl et al. [71] were in the 7–60$\mu\mathrm{mol\,dm^{-3}}$ range.

As a result, both 14-3-3 γ and 14-3-3 η, having the highest affinities to the 14-3-3 binding motifs of CCNY, were used for the next experiments. Furthermore, the assumption that 14-3-3 proteins bind only the phosphorylated 14-3-3 binding motifs of CCNY was confirmed (the binding affinities of the 14-3-3 isoforms to the unphosphorylated S100 peptide were unmeasurable, Fig. 12 C. on page 60).

As a next step, all proteins studied were needed to be prepared in a sufficient amount and quality for biophysical characterization. To understand the mechanisms that occur in cells, wild-type constructs of human 14-3-3 protein isoforms and human CDK16 were used. The preparation of the CCNY construct was more complicated. For the experiments, the pS100 and pS326 CCNY was necessary. However, bacterial cells lack post-translational modifications, including phosphorylation. Therefore, CCNY had to be phosphorylated in vitro, using a specific protein kinase. For this purpose, a CCNY mutant containing three mutations (Y98R, S99A, S324A) was used. These mutations formed PKA phosphorylation sites at residues S100 and S236 that are required 14-3-3 protein binding sites. For the expression and purification of all proteins, the protocols optimized in our laboratory were used. 14-3-3 isoforms, which are produced routinely in our laboratory, are abundant in cells, easily soluble, and produced in high amounts. On the contrary, both CDK16 and CCNY were produced in smaller amounts and tended to precipitation. However, as a result, all proteins were produced in the amount and purity necessary for further experiments (Figs. 15 on page 63, 18 on page 65, 20 on page 67, and 22 on page 69). In addition, CCNY was phosphorylated using PKA (Fig. 21 on page 68).

The interactions between the whole CCNY molecule and both 14-3-3 η and 14-

3-3 γ isoforms were studied using native electrophoresis. The results presented in Figs. 23 A. and B. on page 70 are in agreement with the data from the fluorescence anisotropy measurements. Unphosphorylated CCNY bound neither 14-3-3 η nor 14-3-3 γ, whereas pCCNY bound both of them. These results were the same for both the 1 : 1 and 1 : 2 ratios of the (p)CCNY : 14-3-3 isoform. The results support the hypothesis that the previously reported interaction of pCCNY with 14-3-3 proteins is indeed a prerequisite for CDK16 activation. [5]

The formation of binary pCCNY–14-3-3 and ternary CDK16–pCCNY–14-3-3 protein complexes was studied by size exclusion chromatography. In addition to the results of Shetata et al. [5] who described the common presence of CDK16, pCCNY and 14-3-3 proteins in mouse brain lysates, we discovered that the bacterially expressed CDK16, pCCNY and 14-3-3 proteins formed a ternary complex in vitro (Fig. 25 on page 73). In the sample containing only pCCNY and 14-3-3 proteins, the formation of a binary pCCNY–14-3-3 protein complex was observed (Fig. 24 on page 72). In the size exclusion of the ternary complex (Fig. 25 on page 73), a small amount of unbound CDK16 was observed. This leads to the hypothesis that the binary pCCNY-14-3-3 protein complex is more stable compared to the ternary complex. However, the stability of both complexes will be studied by analytical ultracentrifugation in the near future.

In addition, a last aim of the thesis was the refinement of the crystal structure of the 14-3-3 binding motif of CCNY bound to 14-3-3 γ. The crystal structure was solved with the final resolution 2.201 Å and multiple polar contacts between the phosphopeptide and the 14-3-3 protein were observed (Fig. 26 D. on page 75). These contacts are very similar to those observed in other 14-3-3 protein complexes with phosphopeptides. [71, 72, 73]

The results presented in this thesis identified 14-3-3 η and 14-3-3 γ as the 14-3-3 isoforms that bind CCNY with the highest affinities. It was also shown that pCCNY interacts with 14-3-3 proteins, forming a binary complex, where the unphosphorylated CCNY does not bind at all. Furthermore, CDK16 was found to form a ternary complex with pCCNY and 14-3-3 proteins. The refined crystal structure of 14-3-3 γ with 14-3-3 binding motif of CCNY provides a detailed insight into the interactions at the protein-phosphopeptide interface. Although the exact molecular mechanism of CDK16 activation is still unclear and has to be further investigated by future experiments, the results presented in this thesis can be used as first steps towards understanding the structure and interactions in the CDK16–pCCNY–14-3-3 protein complex.

Conclusion

1. The binding affinities of all human 14-3-3 isoforms for 14-3-3 binding motifs of human CCNY using the fluorescence anisotropy measurements were comapred. As a result, 14-3-3 η and 14-3-3 γ isoforms, binding to the peptides with the highest affinities, were chosen for the next experiments.

2. All selected 14-3-3 isoforms, CCNY and CDK16 were expressed and purified in sufficient amount and purity for biophysical characterization.

3. CCNY was phosphorylated using PKA.

4. The pCCNY–14-3-3 protein interaction was characterized by native electrophoresis. The formation of pCCNY–14-3-3 protein complexes was observed, whereas the unphosphorylated CCNY does not bind any of the used 14-3-3 isoforms.

5. The pCCNY–14-3-3 γ and CDK16–pCCNY–14-3-3 γ complexes were characterized using size exclusion chromatography. In both cases, the formation of binary and ternary complexes was observed.

6. The crystal structure of the 14-3-3 binding motif `RKRSApSADNL` of CCNY bound to 14-3-3 γ was refined and the polar contacts were identified at the protein-peptide interface.

Appendices

Table A.1. Sequence and parameters of CCNY_pS100 peptide for the fluorescence anisotropy measurements

Peptide parameters	
Sequence	H-ARKYSpSCSTIF-OH
Molar mass	$1342.4\,\mathrm{g\,mol^{-1}}$
Purity	96.4 %

Table A.2. Sequence and parameters of CCNY_pS326 peptide for the fluorescence anisotropy measurements

Peptide parameters	
Sequence	H-RKRSApSADNLT-OH
Molar mass	$1298.3\,\mathrm{g\,mol^{-1}}$
Purity	98.7 %

Table A.3. Sequence and parameters of FLC-CCNY_S100 peptide for the fluorescence anisotropy measurements

Peptide parameters	
Sequence	5-Fam-AhxARKYSSCSTIF-OH
Molar mass	$1733.9\,\mathrm{g\,mol^{-1}}$
Purity	97.5 %

Table A.4. Sequence of human 14-3-3 η with N-terminal polyhistidine fusion anchor. *Cleavage site is visualised by underlining.*

10	20	30	40	50	60
MGSSHHHHHH	SSGENLYFQG	HMGDREQLLQ	RARLAEQAER	YDDMASAMKA	VTELNEPLSN
70	80	90	100	110	120
EDRNLLSVAY	KNVVGARRSS	WRVISSIEQK	TMADGNEKKL	EKVKAYREKI	EKELETVCND
130	140	150	160	170	180
VLSLLDKFLI	KNCNDFQYES	KVFYLKMKGD	YYRYLAEVAS	GEKKNSVVEA	SEAAYKEAFE
190	200	210	220	230	240
ISKEQMQPTH	PIRLGLALNF	SVFYYEIQNA	PEQACLLAKQ	AFDDAIAELD	TLNEDSYKDS
250	260				
TLIMQLLRDN	LTLWTSDQQD	EEAGEGN			

Table A.5. Sequence of cleaved human 14-3-3 η. *Cleavage site is visualised by underlining.*

10	20	30	40	50	60
GHMGDREQLL	QRARLAEQAE	RYDDMASAMK	AVTELNEPLS	NEDRNLLSVA	YKNVVGARRS
70	80	90	100	110	120
SWRVISSIEQ	KTMADGNEKK	LEKVKAYREK	IEKELETVCN	DVLSLLDKFL	IKNCNDFQYE
130	140	150	160	170	180
SKVFYLKMKG	DYYRYLAEVA	SGEKKNSVVE	ASEAAYKEAF	EISKEQMQPT	HPIRLGLALN
190	200	210	220	230	240
FSVFYYEIQN	APEQACLLAK	QAFDDAIAEL	DTLNEDSYKD	STLIMQLLRD	NLTLWTSDQQ

DEEAGEGN

Table A.6. 14-3-3 η parameters (computed by ProtParam [74])

	Before cleavage	After cleavage
Number of amino acids	267	248
Molar mass	30.6 kDa	28.4 kDa
Theoretical pI	5.1	4.8
Extinction coefficient	30370 μmol dm^{-3}	28880 g mol^{-1}

Table A.7. Sequence of human 14-3-3 γ with N-terminal polyhistidine fusion anchor. *Cleavage site is visualised by underlining.*

10	20	30	40	50	60
MGSSHHHHHH	SSGENLYFQG	HMVDREQLVQ	KARLAEQAER	YDDMAAAMKN	VTELNEPLSN
70	80	90	100	110	120
EERNLLSVAY	KNVVGARRSS	WRVISSIEQK	TSADGNEKKI	EMVRAYREKI	EKELEAVCQD
130	140	150	160	170	180
VLSLLDNYLI	KNCSETQYES	KVFYLKMKGD	YYRYLAEVAT	GEKRATVVES	SEKAYSEAHE
190	200	210	220	230	240
ISKEHMQPTH	PIRLGLALNY	SVFYYEIQNA	PEQACHLAKT	AFDDAIAELD	TLNEDSYKDS
250	260				
TLIMQLLRDN	LTLWTSDQQD	DDGGEGNN			

Table A.8. Sequence of cleaved human 14-3-3 γ. *Cleavage site is visualised by underlining.*

```
        10          20          30          40          50          60
GHMVDREQLV  QKARLAEQAE  RYDDMAAAMK  NVTELNEPLS  NEERNLLSVA  YKNVVGARRS
        70          80          90         100         110         120
SWRVISSIEQ  KTSADGNEKK  IEMVRAYREK  IEKELEAVCQ  DVLSLLDNYL  IKNCSETQYE
       130         140         150         160         170         180
SKVFYLKMKG  DYYRYLAEVA  TGEKRATVVE  SSEKAYSEAH  EISKEHMQPT  HPIRLGLALN
       190         200         210         220         230         240
YSVFYYEIQN  APEQACHLAK  TAFDDAIAEL  DTLNEDSYKD  STLIMQLLRD  NLTLWTSDQQ

DDDGGEGNN
```

Table A.9. 14-3-3 γ parameters (computed by ProtParam [74])

	Before cleavage	After cleavage
Number of amino acids	268	249
Molar mass	30.7 kDa	28.5 kDa
Theoretical pI	5.1	4.9
Extinction coefficient	33350 μmol dm^{-3}	31860 g mol^{-1}

Table A.10. Sequence of human cyclin Y (1–341, Y98R, S99A, S324A) with N-terminal glutathione S-transferase fusion anchor. *Cleavage site is visualised by underlining.*

```
        10          20          30          40          50          60
MSPILGYWKI  KGLVQPTRLL  LEYLEEKYEE  HLYERDEGDK  WRNKKFELGL  EFPNLPYYID
        70          80          90         100         110         120
GDVKLTQSMA  IIRYIADKHN  MLGGCPKERA  EISMLEGAVL  DIRYGVSRIA  YSKDFETLKV
       130         140         150         160         170         180
DFLSKLPEML  KMFEDRLCHK  TYLNGDHVTH  PDFMLYDALD  VVLYMDPMCL  DAFPKLVCFK
       190         200         210         220         230         240
KRIEAIPQID  KYLKSSKYIA  WPLQGWQATF  GGGDHPPKSD  LEVLFQGPLG  SMGNTTSCCV
       250         260         270         280         290         300
SSSPKLRRNA  HSRLESYRPD  TDLSREDTGC  NLQHISDREN  IDDLNMEFNP  SDHPRASTIF
       310         320         330         340         350         360
LSKSQTDVRE  KRKSLFINHH  PPGQIARKRA  SCSTIFLDDS  TVSQPNLKYT  IKCVALAIYY
       370         380         390         400         410         420
HIKNRDPDGR  MLLDIFDENL  HPLSKSEVPP  DYDKHNPEQK  QIYRFVRTLF  SAAQLTAECA
       430         440         450         460         470         480
IVTLVYLERL  LTYAEIDICP  ANWKRIVLGA  ILLASKVWDD  QAVWNVDYCQ  ILKDITVEDM
       490         500         510         520         530         540
NELERQFLEL  LQFNINVPSS  VYAKYYFDLR  SLAEANNLSF  PLEPLSRERA  HKLEAISRLC
       550         560         570
EDKYKDLRRS  ARKRAASADN  LTLPRWSPAI  IS
```

Table A.11. Sequence of human cyclin Y (1–341, Y98R, S99A, S324A) after cleavage. *Cleavage site is visualised by underlining.*

10	20	30	40	50	60
GPLGSMGNTT	SCCVSSSPKL	RRNAHSRLES	YRPDTDLSRE	DTGCNLQHIS	DRENIDDLNM
70	80	90	100	110	120
EFNPSDHPRA	STIFLSKSQT	DVREKRKSLF	INHHPPGQIA	RKRASCSTIF	LDDSTVSQPN
130	140	150	160	170	180
LKYTIKCVAL	AIYYHIKNRD	PDGRMLLDIF	DENLHPLSKS	EVPPDYDKHN	PEQKQIYRFV
190	200	210	220	230	240
RTLFSAAQLT	AECAIVTLVY	LERLLTYAEI	DICPANWKRI	VLGAILLASK	VWDDQAVWNV
250	260	270	280	290	300
DYCQILKDIT	VEDMNELERQ	FLELLQFNIN	VPSSVYAKYY	FDLRSLAEAN	NLSFPLEPLS
310	320	330	340		
RERAHKLEAI	SRLCEDKYKD	LRRSARKRAA	SADNLTLPRW	SPAIIS	

Table A.12. Cyclin Y (1–341, Y98R, S99A, S324A) parameters (computed by ProtParam [74])

	Before cleavage	After cleavage
Number of amino acids	572	346
Molar mass	66.1 kDa	39.7 kDa
Theoretical pI	6.3	7.2
Extinction coefficient	84230 $\mathrm{g\,mol^{-1}}$	41370 $\mathrm{g\,mol^{-1}}$

Table A.13. Sequence of human CDK16 (1–496) with N-terminal glutathione S-transferase fusion anchor. *Cleavage site is visualised by underlining.*

```
        10          20          30          40          50          60
MSPILGYWKI  KGLVQPTRLL  LEYLEEKYEE  HLYERDEGDK  WRNKKFELGL  EFPNLPYYID
        70          80          90         100         110         120
GDVKLTQSMA  IIRYIADKHN  MLGGCPKERA  EISMLEGAVL  DIRYGVSRIA  YSKDFETLKV
       130         140         150         160         170         180
DFLSKLPEML  KMFEDRLCHK  TYLNGDHVTH  PDFMLYDALD  VVLYMDPMCL  DAFPKLVCFK
       190         200         210         220         230         240
KRIEAIPQID  KYLKSSKYIA  WPLQGWQATF  GGGDHPPKSD  LEVLFQGPLG  SMDRMKKIKR
       250         260         270         280         290         300
QLSMTLRGGR  GIDKTNGAPE  QIGLDESGGG  GGSDPGEAPT  RAAPGELRSA  RGPLSSAPEI
       310         320         330         340         350         360
VHEDLKMGSD  GESDQASATS  SDEVQSPVRV  RMRNHPPRKI  STEDINKRLS  LPADIRLPEG
       370         380         390         400         410         420
YLEKLTLNSP  IFDKPLSRRL  RRVSLSEIGF  GKLETYIKLD  KLGEGTYATV  YKGKSKLTDN
       430         440         450         460         470         480
LVALKEIRLE  HEEGAPCTAI  REVSLLKDLK  HANIVTLHDI  IHTEKSLTLV  FEYLDKDLKQ
       490         500         510         520         530         540
YLDDCGNIIN  MHNVKLFLFQ  LLRGLAYCHR  QKVLHRDLKP  QNLLINERGE  LKLADFGLAR
       550         560         570         580         590         600
AKSIPTKTYS  NEVVTLWYRP  PDILLGSTDY  STQIDMWGVG  CIFYEMATGR  PLFPGSTVEE
       610         620         630         640         650         660
QLHFIFRILG  TPTEETWPGI  LSNEEFKTYN  YPKYRAEALL  SHAPRLDSDG  ADLLTKLLQF
       670         680         690         700         710         720
EGRNRISAED  AMKHPFFLSL  GERIHKLPDT  TSIFALKEIQ  LQKEASLRSS  SMPDSGRPAF

RVVDTEF
```

Table A.14. Sequence of cleaved human CDK16 (1–496). *Cleavage site is visualised by underlining.*

10	20	30	40	50	60
GPLGSMDRMK	KIKRQLSMTL	RGGRGIDKTN	GAPEQIGLDE	SGGGGGSDPG	EAPTRAAPGE
70	80	90	100	110	120
LRSARGPLSS	APEIVHEDLK	MGSDGESDQA	SATSSDEVQS	PVRVRMRNHP	PRKISTEDIN
130	140	150	160	170	180
KRLSLPADIR	LPEGYLEKLT	LNSPIFDKPL	SRRLRRVSLS	EIGFGKLETY	IKLDKLGEGT
190	200	210	220	230	240
YATVYKGKSK	LTDNLVALKE	IRLEHEEGAP	CTAIREVSLL	KDLKHANIVT	LHDIIHTEKS
250	260	270	280	290	300
LTLVFEYLDK	DLKQYLDDCG	NIINMHNVKL	FLFQLLRGLA	YCHRQKVLHR	DLKPQNLLIN
310	320	330	340	350	360
ERGELKLADF	GLARAKSIPT	KTYSNEVVTL	WYRPPDILLG	STDYSTQIDM	WGVGCIFYEM
370	380	390	400	410	420
ATGRPLFPGS	TVEEQLHFIF	RILGTPTEET	WPGILSNEEF	KTYNYPKYRA	EALLSHAPRL
430	440	450	460	470	480
DSDGADLLTK	LLQFEGRNRI	SAEDAMKHPF	FLSLGERIHK	LPDTTSIFAL	KEIQLQKEAS
490	500				
LRSSSMPDSG	RPAFRVVDTE	F			

Table A.15. CDK16 (1–496) parameters (computed by ProtParam [74])

	Before cleavage	After cleavage
Number of amino acids	727	501
Molar mass	82.5 kDa	56.1 kDa
Theoretical pI	6.4	7.3
Extinction coefficient	80220 $\mathrm{g\,mol^{-1}}$	37360 $\mathrm{g\,mol^{-1}}$

Table A.16. LB medium

Buffer contents	
tryptone	10 $\mathrm{g\,l^{-1}}$
NaCl	10 $\mathrm{g\,l^{-1}}$
yeast extract	5 $\mathrm{g\,l^{-1}}$

Table A.17. 10× PBS buffer

Buffer contents	
NaCl	80 $\mathrm{g\,l^{-1}}$
KCl	2 $\mathrm{g\,l^{-1}}$
KH_2PO_4	2.4 $\mathrm{g\,l^{-1}}$
$NaHPO_4 \cdot 2\,H_2O$	14.4 $\mathrm{g\,l^{-1}}$
NaN_3	0.4 $\mathrm{g\,l^{-1}}$

Table A.18. 5× sampling buffer. *Contents for 10 ml.*

Buffer contents	
1mol dm^{-3} Tris-HCl pH 6.8	0.6 ml
50% glycerol	5 ml
10% SDS	2 ml
β-mercaptoethanol	0.5 ml
1% bromophenol blue	1 ml
H_2O	0.9 ml

Table A.19. SDS gel. *Ccontents for 2 gels.*

Separating gel contents	
Acrylamide/Bis-acrylamide (Tab. A.20)	5.625 ml
4× separating buffer (Tab. A.21)	3 ml
H_2O	2.625 ml
APS	67.5 μl
TEMED	7.5 μl
Resolving gel contents	
Acrylamide/bis-acrylamide (Tab. A.20)	0.5 ml
4× resolving buffer (Tab. A.22)	1 ml
H_2O	2.25 ml
APS	45 μl
TEMED	5 μl

Table A.20. Acrylamide/Bis-acrylamide *Contents for 100 ml.*

Buffer contents	
Acrylamide	29.2 g
Bis-acrylamide	0.8 g
H_2O	to 100 ml

Table A.21. 4× separating buffer. *Contents for 100 ml.*

Buffer contents	
2mol dm^{-3} Tris-HCl pH 8.8	75 ml
10% SDS	4 ml
H_2O	21 ml

Table A.22. 4× resolving buffer. *Contents for 100 ml.*

Buffer contents	
1mol dm^{-3} Tris-HCl pH 6.8	50 ml
10% SDS	4 ml
H_2O	46 ml

Table A.23. Staining dye. *Contents for 1 liter.*

Dye contents	
Coomassie Brilliant Blue R 250	1 g
methanol	450 ml
acetic acid	100 ml

Table A.24. 12% native PAGE gel. *Contents for 1 gel.*

Gel contents	
Rotiphorese Gel 30	3.4 ml
10× TBE buffer (Tab. XX on page 50)	0.6 ml
H_2O	2.97 ml
APS	30 µl
TEMED	7.5 µl

Table A.25. Sampling buffer for native PAGE. *Contents for 10 ml.*

Buffer contents	
10× TBE buffer (Tab. XX on page 50)	1 ml
bromophenol blue	10 mg
glycerol	3 ml
H_2O	to 10 ml

References

[1] R. Sender, S. Fuchs, and R. Milo. Revised Estimates for the Number of Human and Bacteria Cells in the Body. *PLOS Biology*, 14(8):e1002533, August 2016.

[2] G. Krauss. *Biochemistry of signal transduction and regulation*. Wiley-VCH, Weinheim, 5., completely rev. edition, 2014. OCLC: 877912163.

[3] D. L. Nelson. *Lehninger principles of biochemistry*. Macmillan International Higher Education., New York, NY, 8th edition, 2021.

[4] M. Malumbres. Cyclin-dependent kinases. *Genome Biology*, 15(6):122, 2014.

[5] S. N. Shehata, M. Deak, N. A. Morrice, E. Ohta, R. W. Hunter, V. M. Kalscheuer, and K. Sakamoto. Cyclin Y phosphorylation- and 14-3-3-binding-dependent activation of PCTAIRE-1/CDK16. *Biochemical Journal*, 469(3):409–420, August 2015.

[6] P. Mikolcevic, R. Sigl, V. Rauch, M. W. Hess, K. Pfaller, M. Barisic, L. J. Pelliniemi, M. Boesl, and S. Geley. Cyclin-dependent kinase 16/PCTAIRE kinase 1 is activated by cyclin Y and is essential for spermatogenesis. *Molecular and Cellular Biology*, 32(4):868–879, February 2012.

[7] Z. Wang. Regulation of Cell Cycle Progression by Growth Factor-Induced Cell Signaling. *Cells*, 10(12):3327, November 2021.

[8] W. Stallaert, K. M. Kedziora, H. X. Chao, and J. E. Purvis. Bistable switches as integrators and actuators during cell cycle progression. *FEBS Letters*, 593(20):2805–2816, October 2019.

[9] E. S. Wenzel and T. K. S. Amareshwar. Cell-cycle Checkpoints and Aneuploidy on the Path to Cancer. *In Vivo*, 32(1), January 2018.

[10] P. Icard, L. Fournel, Z. Wu, M. Alifano, and H. Lincet. Interconnection between Metabolism and Cell Cycle in Cancer. *Trends in Biochemical Sciences*, 44(6):490–501, June 2019.

[11] M. Malumbres and M. Barbacid. Cell cycle, CDKs and cancer: a changing paradigm. *Nature Reviews. Cancer*, 9(3):153–166, March 2009.

[12] S. S. Taylor and A. P. Kornev. Protein kinases: evolution of dynamic regulatory proteins. *Trends in Biochemical Sciences*, 36(2):65–77, February 2011.

[13] C. Arter, L. Trask, S. Ward, S. Yeoh, and R. Bayliss. Structural features of the protein kinase domain and targeted binding by small-molecule inhibitors. *Journal of Biological Chemistry*, 298(8):102247, August 2022.

[14] D. Bossemeyer. Protein kinases - structure and function. *FEBS Letters*, 369(1):57–61, August 1995.

[15] A. R. Nebreda. CDK activation by non-cyclin proteins. *Current Opinion in Cell Biology*, 18(2):192–198, April 2006.

[16] D. Santamaría, C. Barrière, A. Cerqueira, S. Hunt, C. Tardy, K. Newton, J. F. Cáceres, P. Dubus, M. Malumbres, and M. Barbacid. Cdk1 is sufficient to drive the mammalian cell cycle. *Nature*, 448(7155):811–815, August 2007.

[17] N. J. Tatum and J. A. Endicott. Chatterboxes: the structural and functional diversity of cyclins. *Seminars in Cell & Developmental Biology*, 107:4–20, November 2020.

[18] P. Mikolcevic, J. Rainer, and S. Geley. Orphan kinases turn eccentric: a new class of cyclin Y-activated, membrane-targeted CDKs. *Cell Cycle (Georgetown, Tex.)*, 11(20):3758–3768, October 2012.

[19] M. E. M. Noble, J. A. Endicott, N. R. Brown, and L. N. Johnson. The cyclin box fold: protein recognition in cell-cycle and transcription control. *Trends in Biochemical Sciences*, 22(12):482–487, December 1997.

[20] J. A. Coffman. Cell Cycle Development. *Developmental Cell*, 6(3):321–327, March 2004.

[21] M. Huse and J. Kuriyan. The conformational plasticity of protein kinases. *Cell*, 109(3):275–282, May 2002.

[22] D. J. Wood and J. A. Endicott. Structural insights into the functional diversity of the CDK–cyclin family. *Open Biology*, 8(9):180112, September 2018.

[23] S. E. Dixon-Clarke, S. N. Shehata, T. Krojer, T. D. Sharpe, F. Von Delft, K. Sakamoto, and A. N. Bullock. Structure and inhibitor specificity of the PCTAIRE-family kinase CDK16. *Biochemical Journal*, 474(5):699–713, March 2017.

[24] R. Graeser, J. Gannon, R. Y. C. Poon, T. Dubois, A. Aitken, and T. Hunt. Regulation of the CDK-related protein kinase PCTAIRE-1 and its possible role in neurite outgrowth in Neuro-2A cells. *Journal of Cell Science*, 115(Pt 17):3479–3490, September 2002.

[25] S. N. Shehata, M. Deak, C. Collodet, S. F. Spiegl, S. Geley, D. Sumpton, and K. Sakamoto. Identification of novel PCTAIRE-1/CDK16 substrates using a chemical genetic screen. *Cellular Signalling*, 59:53–61, July 2019.

[26] Ch. Y. Ou, V. Y. Poon, C. I. Maeder, S. Watanabe, E. K. Lehrman, A. K. Y. Fu, M. Park, W. Y. Fu, E. M. Jorgensen, N. Y. Ip, and K. Shen. Two Cyclin-Dependent Kinase Pathways Are Essential for Polarized Trafficking of Presynaptic Components. *Cell*, 141(5):846–858, May 2010.

[27] H. Hu, S. A. Haas, J. Chelly, H. Van Esch, M. Raynaud, and A. P. M. et al. De Brouwer. X-exome sequencing of 405 unresolved families identifies seven novel intellectual disability genes. *Molecular Psychiatry*, 21(1):133–148, January 2016.

[28] S. Charrasse, I. Carena, J. Hagmann, K. Woods-Cook, and S. Ferrari. PCTAIRE-1: characterization, subcellular distribution, and cell cycle-dependent kinase activity. *Cell Growth & Differentiation: The Molecular Biology Journal of the American Association for Cancer Research*, 10(9):611–620, September 1999.

[29] S. Li, M. Jiang, W. Wang, and J. Chen. 14-3-3 Binding to Cyclin Y contributes to cyclin Y/CDK14 association. *Acta Biochimica et Biophysica Sinica*, 46(4):299–304, April 2014.

[30] D. Liu and R. L. Finley. Cyclin Y Is a Novel Conserved Cyclin Essential for Development in Drosophila. *Genetics*, 184(4):1025–1035, April 2010.

[31] X. Li, J. Li, L. Xu, W. Wei, A. Cheng, L. Zhang, M. Zhang, G. Wu, and Ch. Cai. CDK16 promotes the progression and metastasis of triple-negative breast cancer by phosphorylating PRC1. *Journal of experimental & clinical cancer research: CR*, 41(1):149, April 2022.

[32] B. W. Moore, V. J. Perez, and F. D. Carlson. Specific acidic proteins of the nervous system in physiological and biochemical aspects of nervous integration. *Englewood Cliffs, NJ: Prentice-Hall*, pages 343–359, 1967.

[33] M. Rosenquist, P. Sehnke, R. J. Ferl, M. Sommarin, and Ch. Larsson. Evolution of the 14-3-3 Protein Family: Does the Large Number of Isoforms in Multicellu-

lar Organisms Reflect Functional Specificity? *Journal of Molecular Evolution*, 51(5):446–458, November 2000.

[34] A. Aitken, S. Howell, D. Jones, J. Madrazo, and Y. Patel. 14-3-3 alpha and delta are the phosphorylated forms of raf-activating 14-3-3 beta and zeta. In vivo stoichiometric phosphorylation in brain at a Ser-Pro-Glu-Lys MOTIF. *The Journal of Biological Chemistry*, 270(11):5706–5709, March 1995.

[35] T. Ichimura, T. Isobe, T. Okuyama, N. Takahashi, K. Araki, R. Kuwano, and Y. Takahashi. Molecular cloning of cDNA coding for brain-specific 14-3-3 protein, a protein kinase-dependent activator of tyrosine and tryptophan hydroxylases. *Proceedings of the National Academy of Sciences of the United States of America*, 85(19):7084–7088, October 1988.

[36] V. Obsilova and T. Obsil. The 14-3-3 Proteins as Important Allosteric Regulators of Protein Kinases. *International Journal of Molecular Sciences*, 21(22):8824, November 2020.

[37] G. P. H. van Heusden and H. Y. Steensma. Yeast 14-3-3 proteins. *Yeast (Chichester, England)*, 23(3):159–171, February 2006.

[38] M. Rosenquist, M. Alsterfjord, C. Larsson, and M. Sommarin. Data mining the Arabidopsis genome reveals fifteen 14-3-3 genes. Expression is demonstrated for two out of five novel genes. *Plant Physiology*, 127(1):142–149, September 2001.

[39] Y. Xu, J. Ren, X. He, H. Chen, T. Wei, and W. Feng. YWHA/14-3-3 proteins recognize phosphorylated TFEB by a noncanonical mode for controlling TFEB cytoplasmic localization. *Autophagy*, 15(6):1017–1030, June 2019.

[40] J. Liu, S. Cao, G. Ding, B. Wang, Y. Li, Y. Zhao, Q. Shao, J. Feng, S. Liu, L. Qin, and Y. Xiao. The role of 14-3-3 proteins in cell signalling pathways and virus infection. *Journal of Cellular and Molecular Medicine*, 25(9):4173–4182, May 2021.

[41] R. Marais and C. Marshall. 14-3-3 proteins: structure resolved, functions less clear. *Structure (London, England: 1993)*, 3(8):751–753, August 1995.

[42] B. Xiao, S. J. Smerdon, D. H. Jones, G. G. Dodson, Y. Soneji, A. Aitken, and S. J. Gamblin. Structure of a 14-3-3 protein and implications for coordination of multiple signalling pathways. *Nature*, 376(6536):188–191, July 1995.

[43] X. Yang, W. H. Lee, F. Sobott, E. Papagrigoriou, C. V. Robinson, J. G. Grossmann, M. Sundström, D. A. Doyle, and J. M. Elkins. Structural basis for

protein–protein interactions in the 14-3-3 protein family. *Proceedings of the National Academy of Sciences*, 103(46):17237–17242, November 2006.

[44] T. Obsil and V. Obsilova. Structural basis of 14-3-3 protein functions. *Seminars in Cell & Developmental Biology*, 22(7):663–672, September 2011.

[45] N. N. Sluchanko and N. B. Gusev. Oligomeric structure of 14-3-3 protein: What do we know about monomers? *FEBS Letters*, 586(24):4249–4256, December 2012.

[46] A. K. Gardino, S. J. Smerdon, and M. B. Yaffe. Structural determinants of 14-3-3 binding specificities and regulation of subcellular localization of 14-3-3-ligand complexes: A comparison of the X-ray crystal structures of all human 14-3-3 isoforms. *Seminars in Cancer Biology*, 16(3):173–182, June 2006.

[47] M. B. Yaffe, K. Rittinger, S. Volinia, P. R. Caron, A. Aitken, H. Leffers, S. J. Gamblin, S. J. Smerdon, and L. C. Cantley. The Structural Basis for 14-3-3:Phosphopeptide Binding Specificity. *Cell*, 91(7):961–971, December 1997.

[48] B. Kostelecky, A. T. Saurin, A. Purkiss, P. J. Parker, and N. Q. McDonald. Recognition of an intra-chain tandem 14-3-3 binding site within PKCε. *EMBO reports*, 10(9):983–989, September 2009.

[49] D. Bridges and G. B. G. Moorhead. 14-3-3 proteins: a number of functions for a numbered protein. *Science's STKE: signal transduction knowledge environment*, 2005(296):re10, August 2005.

[50] J. M. Woodcock, J. Murphy, F. C. Stomski, M. C. Berndt, and A. F. Lopez. The Dimeric Versus Monomeric Status of 14-3-3ζ Is Controlled by Phosphorylation of Ser58 at the Dimer Interface. *Journal of Biological Chemistry*, 278(38):36323–36327, September 2003.

[51] Z. Trošanová, P. Louša, A. Kozeleková, T. Brom, N. Gašparik, J. Tungli, V. Weisová, E. Župa, G. Žoldák, and J. Hritz. Quantitation of Human 14-3-3 ζ Dimerization and the Effect of Phosphorylation on Dimer-monomer Equilibria. *Journal of Molecular Biology*, 434(7):167479, April 2022.

[52] J. R. Lakowicz. *Principles of fluorescence spectroscopy*. Springer, New York, 3rd edition, 2006.

[53] O. D. Hendrickson, N. A. Taranova, A. V. Zherdev, B. B. Dzantiev, and S. A. Eremin. Fluorescence Polarization-Based Bioassays: New Horizons. *Sensors*, 20(24):7132, December 2020.

[54] E. Hochuli. Purification of Recombinant Proteins with Metal Chelate Adsorbent. In J. K. Setlow, editor, *Genetic Engineering*, pages 87–98. Springer US, Boston, MA, 1990.

[55] K. Wilson and J. M. Walker, editors. *Principles and techniques of biochemistry and molecular biology*. Cambridge University Press, Cambridge, UK : New York, 7th ed edition, 2009. OCLC: ocn463454153.

[56] D. M. Bollag. Ion-Exchange Chromatography. In *Peptide Analysis Protocols*, volume 36, pages 11–22. Humana Press, New Jersey, November 1994.

[57] C. O'Fágáin, P. M. Cummins, and B. F. O'Connor. Gel-filtration chromatography. *Methods in Molecular Biology (Clifton, N.J.)*, 681:25–33, 2011.

[58] H. G. Vikis and K. L. Guan. Glutathione-S-Transferase–Fusion Based Assays for Studying Protein–Protein Interactions. In *Protein-Protein Interactions*, volume 261, pages 175–186. Humana Press, New Jersey, March 2004.

[59] Y. Shi. A Glimpse of Structural Biology through X-Ray Crystallography. *Cell*, 159(5):995–1014, November 2014.

[60] G. Rhodes. *Crystallography made crystal clear: a guide for users of macromolecular models*. Complementary science series. Elsevier/Academic Press, Amsterdam; Boston, 3rd ed edition, 2006. OCLC: ocm62509327.

[61] P. W. Atkins and J. De Paula. *Fyzikální chemie*. Vysoká škola chemicko-technologická v Praze, Praha, 1st edition, 2013. OCLC: 837501815.

[62] M. S. Smyth. x Ray crystallography. *Molecular Pathology*, 53(1):8–14, February 2000.

[63] G. Scapin. Molecular replacement then and now. *Acta Crystallographica Section D Biological Crystallography*, 69(11):2266–2275, November 2013.

[64] P. D. Adams, P. V. Afonine, R. W. Grosse-Kunstleve, R. J. Read, J. Ss Richardson, D. C. Richardson, and T. C. Terwilliger. Recent developments in phasing and structure refinement for macromolecular crystallography. *Current Opinion in Structural Biology*, 19(5):566–572, October 2009.

[65] P. V. Afonine, R. W. Grosse-Kunstleve, N. Echols, J. J. Headd, N. W. Moriarty, M. Mustyakimov, T. C. Terwilliger, A. Urzhumtsev, P. H. Zwart, and P. D. Adams. Towards automated crystallographic structure refinement with *phenix.refine*. *Acta Crystallographica Section D Biological Crystallography*, 68(4):352–367, April 2012.

[66] A. T. Brünger. Free R value: a novel statistical quantity for assessing the accuracy of crystal structures. *Nature*, 355(6359):472–475, January 1992.

[67] D. Liebschner, P. V. Afonine, M. L. Baker, G. Bunkóczi, V. B. Chen, T. I. Croll, B. Hintze, L. Hung, S. Jain, A. J. McCoy, N. W. Moriarty, R. D. Oeffner, B. K. Poon, M. G. Prisant, R. J. Read, J. S. Richardson, D. C. Richardson, M. D. Sammito, O. V. Sobolev, D. H. Stockwell, T. C. Terwilliger, A. G. Urzhumtsev, L. L. Videau, C. J. Williams, and P. D. Adams. Macromolecular structure determination using X-rays, neutrons and electrons: recent developments in *Phenix*. *Acta Crystallographica Section D Structural Biology*, 75(10):861–877, October 2019.

[68] C. J. Williams, J. J. Headd, N. W. Moriarty, M. G. Prisant, L. L. Videau, L. N. Deis, V. Verma, D. A. Keedy, B. J. Hintze, V. B. Chen, S. Jain, S. M. Lewis, W. B. Arendall, J. Snoeyink, P. D. Adams, S. C. Lovell, J. S. Richardson, and D. C. Richardson. MolProbity: More and better reference data for improved all-atom structure validation: PROTEIN SCIENCE.ORG. *Protein Science*, 27(1):293–315, January 2018.

[69] P. Emsley, B. Lohkamp, W. G. Scott, and K. Cowtan. Features and development of *Coot*. *Acta Crystallographica Section D Biological Crystallography*, 66(4):486–501, April 2010.

[70] V. Obsilova, P. Herman, J. Vecer, M. Sulc, J. Teisinger, and Tomas O. 14-3-3ζ C-terminal Stretch Changes Its Conformation upon Ligand Binding and Phosphorylation at Thr232. *Journal of Biological Chemistry*, 279(6):4531–4540, February 2004.

[71] P. Pohl, R. Joshi, O. Petrvalska, T. Obsil, and V. Obsilova. 14-3-3-protein regulates Nedd4-2 by modulating interactions between HECT and WW domains. *Communications Biology*, 4(1):899, July 2021.

[72] D. Kalabova, F. Filandr, M. Alblova, O. Petrvalska, M. Horvath, P. Man, T. Obsil, and V. Obsilova. 14-3-3 protein binding blocks the dimerization interface of caspase-2. *The FEBS Journal*, 287(16):3494–3510, August 2020.

[73] M. Wolter, D. L. Santo, P. Herman, A. Ballone, F. Centorrino, T. Obsil, and C. Ottmann. Interaction of an IκBα Peptide with 14-3-3. *ACS Omega*, 5(10):5380–5388, March 2020.

[74] E. Gasteiger. ExPASy: the proteomics server for in-depth protein knowledge and analysis. *Nucleic Acids Research*, 31(13):3784–3788, July 2003.